2017

An Integrative Synthetic, Spectroscopic, and Computational Study of the Free Radical Chlorine Dioxide and its Interactions with Hydrogen Bonded Networks

Sarah C. Sutton
University of Mississippi. Sally McDonnell Barksdale Honors College

An Integrative Synthetic, Spectroscopic, and Computational Study of the Free Radical Chlorine Dioxide and its Interactions with Hydrogen Bonded Networks

by Sarah Courtney Sutton

A thesis submitted to the faculty of The University of Mississippi in partial fulfillment of the requirements of the Sally McDonnell Barksdale Honors College.

Oxford
May 2017

Approved by

Advisor: Professor Nathan Hammer

Reader: Professor Walter Cleland, Jr.

Reader: Professor Jason Ritchie

ACKNOWLEDGEMENTS

Many people at the University of Mississippi were fundamental in the completion of this thesis. I would like to thank the Sally McDonnell Barksdale Honors College for granting me multiple opportunities to learn inside and outside the traditional classroom setting; this thesis is just one example of the multiple integrative studies I have been able to partake in through the Honors College. I would also like to thank my professors in the Department of Chemistry and Biochemistry for teaching and mentoring me during my tenure at the University of Mississippi. I greatly appreciate the time my professors dedicated to my intellectual and personal growth. I would like to specifically thank Dr. Nathan Hammer for allowing me to conduct research in his group and for investing in my professional development. This research was funded by the

ABSTRACT

SARAH COURTNEY SUTTON: An Integrative Synthetic, Spectroscopic, and Computational Study of the Free Radical Chlorine Dioxide and its Interactions with Hydrogen Bonded Networks
(Under the direction of Dr. Nathan Hammer)

The free radical chlorine dioxide (ClO_2) is a strong oxidizing agent that is used to purify drinking water and medical equipment. The existing literature shows discrepancies in the explanation of the solvent dependent properties of ClO_2. The following thesis investigates these properties by integrating integrates inorganic synthesis, spectroscopic analyses, and computational methods. ClO_2/water hydrogen-bonded networks were computed with the DFT method B3LYP with 6-31G(*d*,*p*) and 6-311++G(2*df*, 2*pd*) basis sets. Raman frequency computations were performed on local minima geometries. Experimental Raman spectra of chlorine dioxide solvated in water and methanol were obtained, and the fundamental symmetric stretch (ν_1) of each spectrum were compared to the computed frequencies. An overall red shift of 12 cm^{-1} for ν_1 was observed in the computational spectra as ClO_2 became more solvated, indicating hydrogen-bond formation between ClO_2 and water. However, no shift was observed in the experimental spectra. This is due to the difference in χ_{ClO2} values for the computations and experiment. However, the experimental value for ν_1 was different in water (945 cm^{-1}) and methanol (940 cm^{-1}) solutions. Also included is an advanced undergraduate laboratory exercise that takes advantage of the unique spectroscopic properties of chlorine dioxide to allow for a direct comparison of its symmetric stretch in both the ground and excited states. Students synthesize aqueous chlorine dioxide, analyze a vibronic progression of the symmetric stretch in the excited state using UV-Vis spectroscopy, and also record the energy of the symmetric stretch in the ground state

using Raman spectroscopy. In addition to offering advanced undergraduate students the opportunity to study the chemistry of a radical first-hand, this exercise also reinforces the use of synthetic techniques for the purpose of studying how a molecule's physical properties vary with the electronic state.

TABLE OF CONTENTS

1 Introduction

1.1 Introduction to the Applications and Properties of Chlorine Dioxide

Chlorine dioxide (ClO_2) has received a considerable amount of attention for its ability to purify drinking water without creating harmful concentrations of disinfection by-products,[1,2] its strong antimicrobial properties,[3] and its ability to oxidize atmospheric ozone.[4] The unique oxidation properties of ClO_2 are believed to be a result of the highly selective nature of one electron-transfer reactions. ClO_2 is a neutral free radical with C_{2v} symmetry and its overall dipole moment is 1.792 Debye.[5] It is known from experiment that ClO_2 has a bent molecular geometry with a bond angle of 117.6°,[6] as shown in Figure 1.1. In its ground state, although the unpaired electron is shared among all three atoms of ClO_2, the majority of the electron density resides mostly on either oxygen atom. The electronegativity of the two oxygen atoms is large enough, in fact, to withdraw electron density from the chlorine atom and give chlorine an induced partial positive charge.

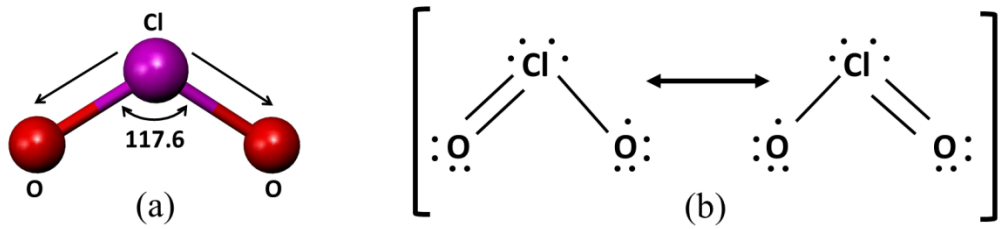

Figure 1.1 (a) ClO2 has a bent conformation. The straight arrows indicate the direction in which the bonds elongate during the symmetric stretch. (b) ClO2 has an unpaired electron

that is shared among all three atoms in two different resonance structures. The unpaired electron mainly resides on one of the oxygen atoms.

Under standard conditions, ClO_2 exists as a yellow gas that can be condensed down into a reddish-brown liquid at 11˚C and solidified to an orange-brown solid at -59˚C. Gaseous ClO_2 is highly soluble in aqueous solutions, remaining unhydrolyzed in its free radical form in the pH range from 2 to 10.[1] It is also relatively easy to synthesize, and it has unique properties inherent to radicals that can be easily studied using optical spectroscopies and computational chemistry.

1.2 Molecular Orbital Theory

1.2.1 Simple Bond Theory

Lewis Electron-Dot Diagrams

The American chemist G.N. Lewis developed a technique to draw molecular bonds based on the valence electrons of the participating atoms. According to Lewis electron-dot theory, a single bond is formed between two atoms that share a pair of electrons. A double bond is formed when two pairs of electrons are shared. A single bond appears on a diagram as a dash between the two participating atoms, and a double bond appears as two dashes. Bonds are formed so atoms can fill their valence shell with eight electrons. This "octet rule" stems from the concept that two electrons are needed to fill up the valence *s* orbital and six electrons are needed to fill up the valence *p* orbital. When an atom has formed enough bonds to satisfy the octet rule, the remaining pairs of electrons that are non-bonding are called a lone pairs. Any unpaired electron is referred to as a radical.

In some instances, a molecule has multiple valid Lewis dot structures, called resonance structures. For example, one double bond can be located between several different atom pairs on the same molecule. Resonance structures must be isoelectric and have nuclei in fixed positions. The resonance structure of ClO_2 in Figure 1b shows the free radical being shared among all three atoms.

Valence Shell Electron-Pair Repulsion

Valence Shell Electron-Pair Repulsion (VSEPR) further characterizes a molecular structure beyond its Lewis dot diagram. VSEPR predicts the structure of a molecule on the basis of electron-electron repulsion. Because electrons are negatively charged, they repel each other. Quantum mechanics dictates that electrons can exist as pairs, but pairs repel other pairs. This repulsion dictates the location of bonds and lone pairs in three-dimensional space. Lone pairs have more concentrated electron density than bonding pairs of electrons. Therefore, repulsion between lone pairs is greater than repulsion between a lone pair and a bonding pair. The repulsion between bonding pairs is less than the repulsion between a lone pair and a bonding pair. The general trend of electron-pair repulsion is clarified below:

lone pair-lone pair > lone pair-bonding pair > bonding pair-bonding pair

The VSEPR model constructs molecular geometries based on steric numbers, or the total number of atoms and lone pairs around a central atom. The number of lone pairs on a molecule dictates its electron geometry. Table 1.1 outlines basic molecular and electron geometries.

Table 1.1 Molecular and electron geometries. (Adapted from *Inorganic Chemistry*[7])

		Number of Lone Pairs		
Steric Number	None	1	2	3
2	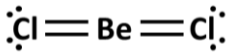			
3	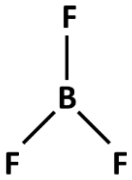	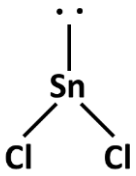		
4	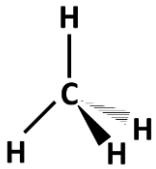	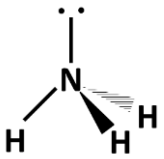	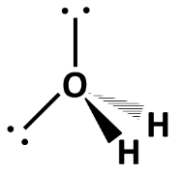	
5	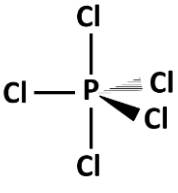	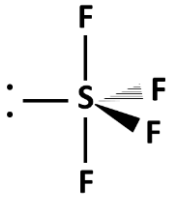	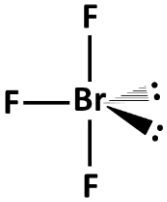	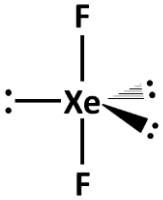

Hydrogen Bonding

In polar solutions, non-bonding interactions between electronegative species (B) and partially positive hydrogen occur. This interaction, called a hydrogen bond, raises the boiling point of solutions and stabilizes macromolecules such as double-helix DNA and protein enzymes. They can be either intermolecular or intramolecular. The strength and character of a hydrogen bond relies on the variation of the following three components:

1. The polarity of X-H (where X is electronegative) creates a dipole moment between the two species. H is partially positive and X is partially negative.

2. A partial covalent bond forms between H···B, causing charge transfer from B to H-X.

3. Dispersion forces effect hydrogen bonds.

Hydrogen bond formation can be detected with infrared or Raman spectroscopy. An IR or Raman active vibrational frequency shifts to a lower frequency upon hydrogen bond formation. This occurs because a hydrogen bond weakens and lengthens the X-H bond. As the X-H bond weakens, the vibrational frequency decreases. The strength of a hydrogen bond can be measured using IR or Raman spectroscopy. These forms of spectroscopy are discussed in Section 1.3.

1.2.2 Symmetry

A molecule's symmetry dictates its electronic structure, spectroscopic properties, and reactivity. Molecules may contain symmetry elements such as mirror planes, inversion centers, or axes of rotations. The process of reflecting, inverting, or rotating is referred to as a symmetry operation. If a molecule is in the exact same position before and after a symmetry operation is performed, then that molecule contains that symmetry element. For example, if a molecule rotated 180˚around its z-axis is in the same location as it was before the rotation, the molecule then possesses an axis of rotation along the z-axis. All

molecules remain unchanged after an identity operation (*E*). Figure 1.2 displays a variety of molecules containing symmetry elements.

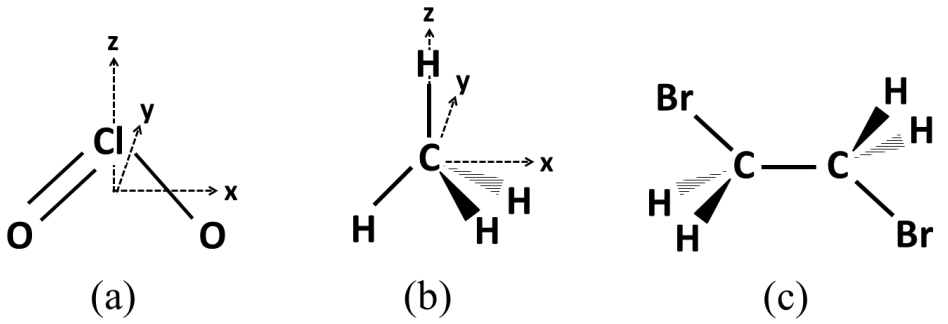

Figure 1.2. The following molecules are: a) chlorine dioxide, b) methanol, and c) 1,2-dibromoethane

Rotation Operations

A rotation operation (C_n) occurs when a molecule is rotated $\frac{360^\circ}{n}$. When the ClO_2 molecule in Figure 1.2 rotates 180˚ around its z-axis, it remains unchanged. Therefore, ClO_2 possesses the rotational element C_2. Methanol (CH_4) contains four C_3 axes, one going down each C-H bond. Molecules may contain several axes of rotation. The axis with the largest *n* value is called the principle axis. Axes perpendicular to the principal axis are designated with a prime. A single prime (C_n') indicates the axis runs through several atoms of the molecule, whereas a double prime (C_n'') indicates the axis runs through the bonds between atoms.

Reflection Operations

A reflection operation (σ) occurs when a molecule has a mirror plane. If a molecule's atoms can be exchanged across a mirror plane axis and remain the same, the molecule contains a reflection element. For example, if the zx-axis of CH_4 was a mirror, the molecule would retain the same image.

Inversions

An inversion (*i*) occurs when atoms are exchanged through the center of a molecule. If the molecule retains its original image, it contains an inversion center. In 1,2-dibromoethane, shown in Figure 2c, Br1 and Br2 can be exchanged without changing the configuration of the molecule.

Rotation-Reflection Operations

A rotation-reflection operation, or improper rotation, involves a rotation followed by a reflection across the axis perpendicular to the axis of rotation. CH_4 contains three S_4 axes, indicated in Figure 1.2b, through the central carbon and between the hydrogen bonds. When CH_4 is rotated 90˚ around its C_4 axis and reflected across the plane perpendicular to the axis, its configuration remains the same.

1.2.3 Point Groups

Because molecules with the same symmetry elements have similar properties, molecules are categorized together based on their symmetry elements. These categories are called point groups. Group theory gives numerical values to symmetry elements within a point group, allowing the properties of point groups to be determined by mathematical methods. Therefore, knowing the point group of a molecule is critical before performing chemical analyses. A series of symmetry operations must be performed in order to deduce a molecule's point group. The flow chart in Figure 1.3 outlines this series.

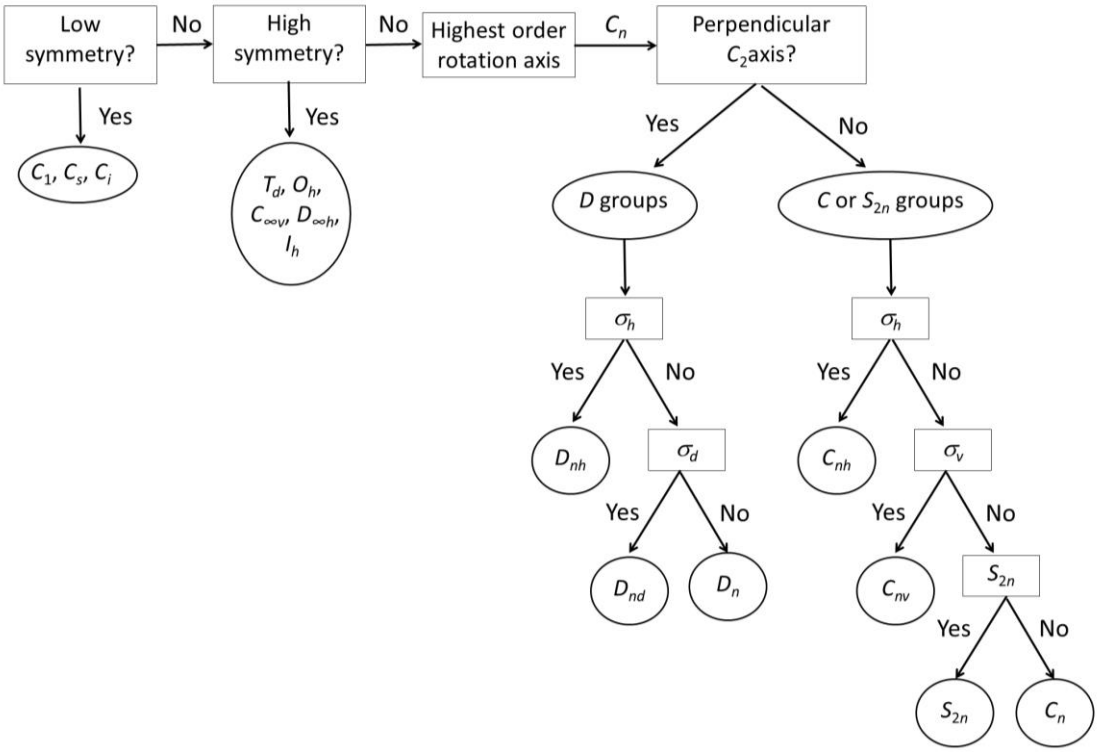

Figure 1.3. This flow chart can be used to determine the point group of a molecule.

(Adapted from *Inorganic Chemistry*[7])

1.2.4 Group Theory

Character tables are created for each point group based on matrices constructed from the locations of atoms in the participating molecule during its point group's symmetry operations. These transformation matrices provide information on the change in the atoms' x, y, and z coordinates after the symmetry operation is performed. The numerical values of these changes are called characters. The C_{2v} character table for ClO_2 is shown in Table 1.2. The sum of all symmetry operations possible for a point group is referred to as the order. The order for the C_{2v} point group is 4. Each column of characters under each symmetry element is called a class. Irreducible representations are

sets, with each row being one set, of characters that are fundamental to every molecule in the C_{2v} point group. Each irreducible representation is labelled by a Mulliken symbol. The label *A*, *B*, *E*, and *T* are used to indicate the symmetry and dimension of the irreducible representation. An irreducible representation with the label *A* is symmetric to the principle rotation axis, whereas the label *B* is antisymmetric to the principle rotation axis. Both of these labels indicate the molecule is singly degenerate, or one dimensional. The label *E* indicates the representation is doubly degenerate, or two dimensional, and the label *T* indicates the representation is triply degenerate, or three dimensional. The subscripts 1 and 2 specify if the representation is symmetric or antisymmetric, respectively, to the C_2 rotation perpendicular to the principle rotation axis. If there is no perpendicular C_2 axis, then the σ_v is used. The subscripts *g* (*gerade*) and *v* (*ungerade*) specify if the irreducible representation is symmetric or antisymmetric, respectively, to inversion. The reducible representation (Γ) is a set of characters that are molecule-dependent.

Table 1.2. The C_2v character table for ClO_2.

C_2v	E	C_2	σ_v(xz)	σ_v' (yz)		
A_1	1	1	1	1	z	x^2, y^2, z^2
A_2	1	1	-1	-1	R_z	xy
B_1	1	-1	1	-1	x, R_y	xz
B_2	1	-1	-1	1	y, R_x	yz
Γ	9	-1	3	1		

Γ is derived from the changes in atoms' location for a specific molecule when a symmetry operation is performed. When a coordinate system is placed on each atom, the

change in axes direction after a symmetry operation is quantified. If the atom is displaced, a 0 is assigned. If the atoms remain in the same positions and its axes do not change direction, a 1 is assigned for every unchanged axis. If the atoms remain in the same position but its axes change direction, a -1 is assigned for every changed axis. For example, when the identity operation (*E*) is performed on ClO_2, all three atoms remain unchanged, and all three axes on each atom remain unchanged. Therefore, the character for Γ under *E* is nine. When ClO_2 is rotated around its principle C_2 axis 180˚, only the Cl atom remains in its original position, and its *x* and *y* axes change direction. The unchanged *z* axis yields a 1, and the flipped *x* and *y* axes yield -1 for each. Therefore, the character for Γ under C_2 is -1. Figure 1.4 further illustrates how to derive Γ for ClO_2.

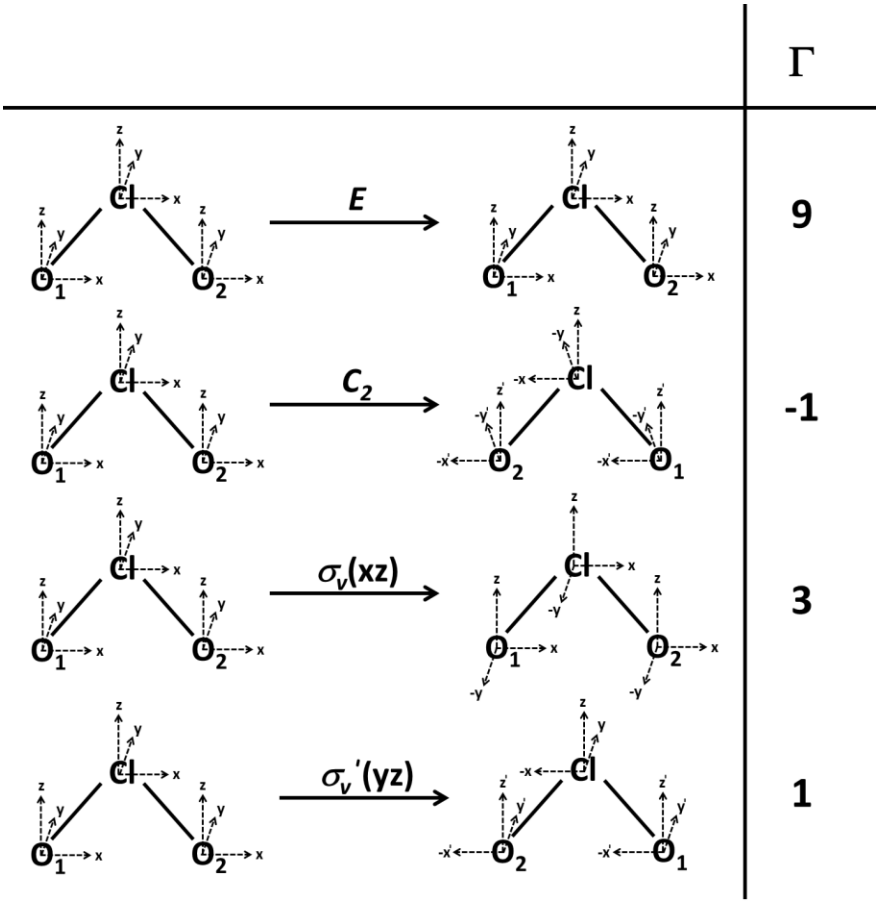

Figure 1.4. Symmetry operations performed on ClO_2 to determine Γ.

Group theory can be used to determine the symmetry of molecular vibrations. The number of vibrations for a molecule can be calculated with Equation 1.1 or 1.2. For *N* number of atoms, there are 3*N* degrees of freedom because there are 3*N* total motions. These motions, or modes, are translational, rotational, or vibrational. A molecule can be displaced in three dimensions (*x*, *y*, or *z*), so three modes are translational. A non-linear molecule can rotate around its *x*, *y*, or *z* axis and still displace atoms. That leaves 3*N* – 6 vibrational modes for *N* number of atoms. A linear molecule can only rotate around its *y* and z axes and still displace atoms. Rotating a linear molecule along its *x*-axis is degenerate. Therefore, only two modes for linear molecules are rotational, leaving 3*N* – 5 vibrational modes. Non-linear ClO_2 has three vibrational modes.

$$\#\ vibrational\ modes\ (non-linear) = 3N - 6 \qquad [1.1]$$

$$\#\ vibrational\ modes\ (linear) = 3N - 5 \qquad [1.2]$$

The number (η) of irreducible representations represented the reducible representation can be calculated with Equation 1.3.

$$\eta = \frac{1}{order}\sum_R \left[\begin{pmatrix} \#operations \\ in\ a\ class \end{pmatrix} \times \begin{pmatrix} character\ of \\ reducible \\ representations \end{pmatrix} \times \begin{pmatrix} character\ of \\ irreducible \\ representation \end{pmatrix} \right] \qquad [1.3]$$

Γ for ClO_2 can then be written as:

$$\Gamma = \eta_{(A1)}A_1 + \eta_{(A2)}A_2 + \eta_{(B1)}B_1 + \eta_{(B1)}B_2$$

$$\Gamma = 2A_1 + B_1$$

The symmetry of each vibrational mode is indicated by each irreducible representation's Mulliken symbol. The 2 A_1 modes are symmetric, whereas the B_1 mode is antisymmetric. The far right columns of the character table are used to determine if a mode is IR or Raman active. Any first-order variable (ex. x) indicates the mode is IR active. Any second-order variable (ex. xy, x^2) indicates the mode is Raman active. All three vibrational modes of ClO_2 are both IR and Raman active.

1.2.5 Molecular Orbital Theory

Molecular orbital theory uses group theory to describe molecular bonds beyond the scope of Lewis electron-dot theory and VSEPR theory. Molecular orbitals are formed when atomic orbitals overlap. Linear combinations of atomic orbitals (LCAO) sum and subtract atomic wavefunctions (ψ) to form the molecular wavefunction (Ψ), shown in Equation 1.4. For atoms *a* and *b*, the coefficients c_a and c_b quantify the contribution of each atomic orbital to the molecular orbital.

$$\Psi = c_a\psi_a + c_b\psi_b \quad [1.4]$$

The wave functions of the molecular orbitals that are formed from the *s* orbitals of atoms *a* and *b* are shown in Equations 1.5 and 1.6. *N* is a normalizing factor, so $\int \Psi\Psi^* \, d\tau = 1$.

$$\Psi = N[c_a\psi_a(1s_a) + c_b\psi_b(1s_b)] \quad [1.5]$$

$$\Psi^* = N[c_a\psi_a(1s_a) - c_b\psi_b(1s_b)] \quad [1.6]$$

Ψ is the wave function of the bonding molecular orbital, and Ψ is the wave function of the antibonding molecular orbital. In an antibonding orbital, the opposing signs of the

atomic orbital wave functions prevent the atomic orbitals from overlapping and forming a molecular bond. The region in between the lobes of an antibonding orbital where no electrons exist is called a node. The energy of a bonding molecular orbital is lower than the energy of an antibonding molecular orbital. The molecular orbital (MO) diagram for a homonuclear diatomic molecule made from *s* orbitals of atoms *a* and *b* is shown in Figure 1.5.

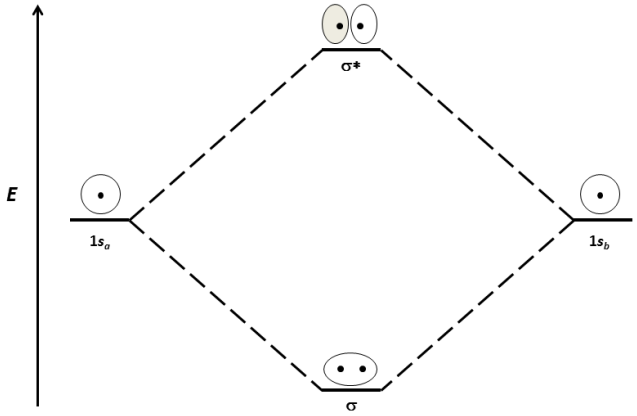

Figure 1.5. The MO diagram of the *s* orbitals of atoms *a* and *b*. (Adapted from *Inorganic Chemistry*[7])

The atomic orbitals of *p* orbitals are more complex because each *p* orbital has two lobes with opposite signs. In order for a molecular orbital to form, two *p* orbital lobes with the same sign must overlap; two lobes of opposing signs cannot overlap. A sigma bond (σ) is formed when two p_z orbitals are subtracted, and a sigma anti-bond (σ^*) is formed when two p_z orbitals are added together. This is illustrated in Figure 1.6a. Pi bonds (π) are formed when p_x or p_y orbitals are added together, and pi anti-bonds (π^*) are formed when p_x or p_y orbitals are subtracted. This is illustrated in Figures 1.6b and 1.6c, respectively. There is a node between the two lobes of the *p* orbital. These nodes are preserved when molecular orbitals form. The molecular orbital diagram of the *p* orbitals of a homonuclear diatomic is shown in Figure 1.7.

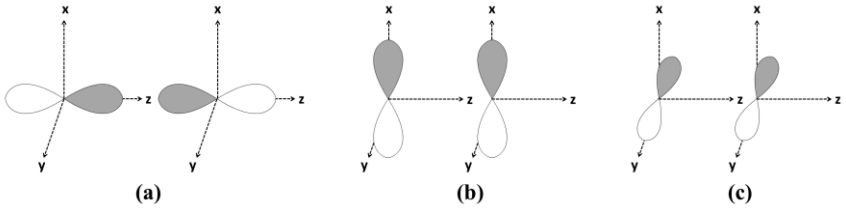

Figure 1.6. (a) p_z orbitals (b) p_x orbitals (c) p_y orbitals.

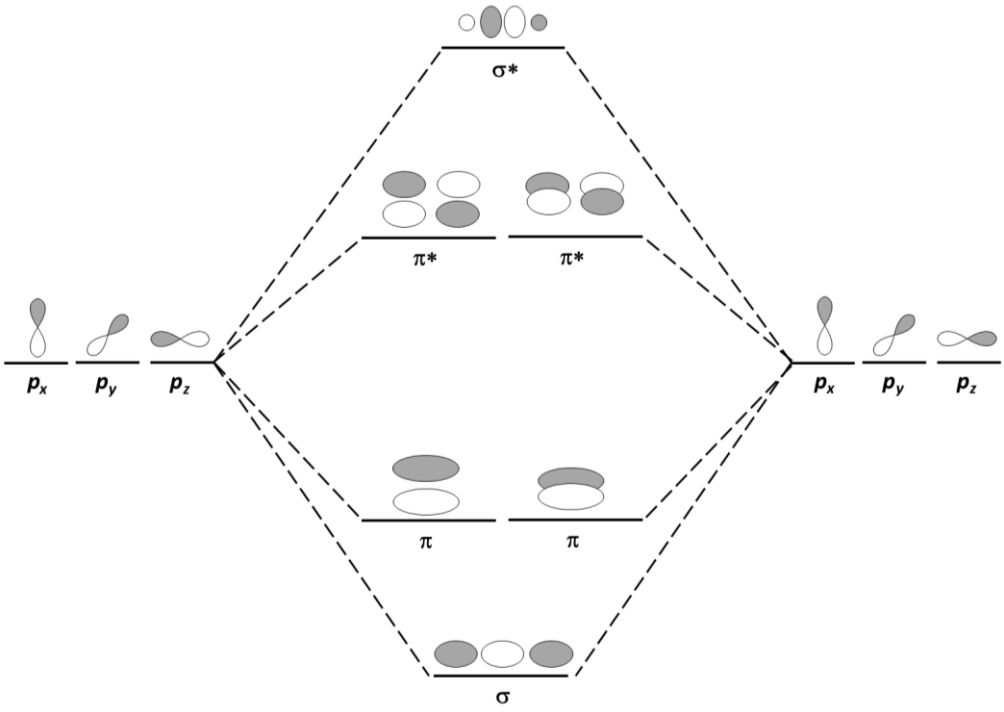

Figure 1.7. The MO diagram of the *p* orbitals of a homonuclear diatomic molecule.

For a molecular orbital diagram of a heteronuclear molecule, the difference in atomic charges causes a difference in the energies of their atomic orbitals. As more electrons are added to an atomic orbital, its atomic orbital potential energy, in eV, becomes more negative. The resulting molecular orbital receives unequal contributions from each atom, and the energy of the resulting molecular orbital shifts. The atomic orbital closer to the molecular orbital contributes more to the molecular orbital.

Occasionally, mixing can occur between σ and σ* levels when both the 2*s* and $2p_z$ orbitals of one atom are similar in energy to the $2p_z$ orbital of the other atom.

The molecular orbital diagram of ClO_2 is shown in Figure 1.7. In order for atomic orbitals to form a bond, they must have the same symmetry. The symmetry of each lobe can be determined by performing the symmetry operations in the molecule's point group. The atomic orbital has the same symmetry as the irreducible representation with the same characters. This process is called finding the symmetry-adapted linear combinations (SALCs) of the orbitals. When all three atomic orbitals have the same symmetry and their lobes are all in phase, a bonding molecular orbital forms. When all three atomic orbitals have the same symmetry but their lobes are not in phase, an antibonding molecular orbital forms. When all three atomic orbitals have the same symmetry but the lobes are unable to overlap, a nonbonding molecular orbital forms.

Molecular orbital diagrams have multiple purposes. The number of bonds formed in a molecule, or its bond order, can be determined using Equation 1.7.

$$Bond\ order = \frac{1}{2}\left[\left(\frac{number\ of}{bonding\ electrons}\right) - \left(\frac{number\ of}{antibonding\ electrons}\right)\right] \qquad [1.7]$$

The bond order for ClO_2 is 1.5, which supports the theory that a double bond is shared among all three atoms. Molecular orbital diagrams also show the frontier orbitals, the highest occupied molecular orbital (HOMO) and the lowest unoccupied molecular orbital (LUMO). These orbitals explain the reaction chemistry of the molecule. For example, the HOMO of ClO_2 is the π* orbital. .

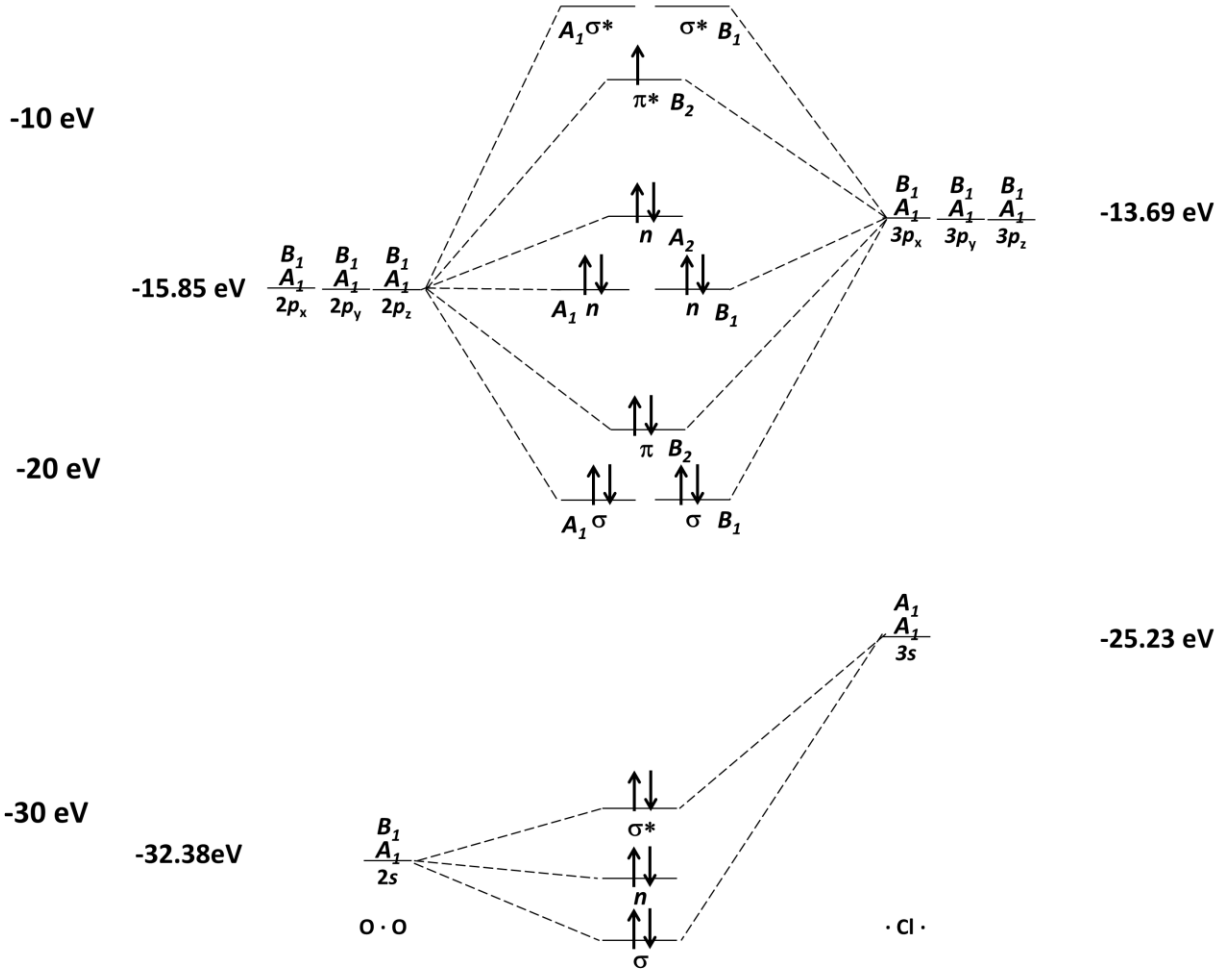

Figure 1.7. The molecular orbital diagram of ClO_2.

1.3 Spectroscopic Methods

1.3.1 Fundamentals of Spectroscopy

Spectroscopy is the study of light and matter interactions and can be used to characterize the physical properties of molecules. Each molecule has quantized translational,

rotational, vibrational, and electronic energy levels. When a molecule is exposed to light of a specific wavelength, a transition between energy levels can occur. In order for a transition to occur, the wavelength of incident light must correspond to an energy that is identical to the energy difference between two levels. Certain spectroscopic methods, such as IR, Raman, and UV-Vis spectroscopy, measure this energy difference.

Quantum mechanical principles are used to characterize a molecule's translational, rotational, vibrational, and electronic energy states. Quantum mechanics postulates the existence of a wavefunction (ψ) that describes the state of the system being studied. A wavefunction is related to the three-dimensional Cartesian coordinates of the system. The probability density, or probability of finding a particle in a three dimensional system, can be calculated using Equation 1.8, where ψ^* is the wavefunction's complex conjugate.

$$P = \int \psi^* \psi d\tau \qquad [1.8]$$

The wavefunction can be found by solving the time-independent Schrodinger equation, shown in Equation 1.9.

$$\hat{H}\psi = E\psi \qquad [1.9]$$

In order to solve the Schrodinger equation for the four different types of energy transitions in molecules, models have been constructed that describe each energetic degree of freedom. The following section will concentrate on the model for vibrational motion, the Harmonic Oscillator.

1.3.2 Vibrational Spectroscopy

The Harmonic Oscillator

Vibrational motion can be described as an object of mass *m* connected to a spring that obeys Hooke's law, shown in Equation 1.10. The force on the spring (F) is directly related to the displacement of the object (x) and the spring constant (k).

$$F = -kx \qquad [1.10]$$

The force is a restoring force because it acts against the direction of displacement. The force is also equal to the negative of the change in potential energy (V) as the object changes position. The equation for the potential energy is shown in Equation 1.11.

$$V = \frac{1}{2}kx^2 \qquad [1.11]$$

The equation for potential energy is parabolic, or harmonic.

Fundamentals of Vibrational Spectroscopy

The vibrational motion of a molecule can be analyzed to characterize its structure. As stated previously, a molecule's vibrational degrees of freedom are represented by atomic displacements known as normal modes. Equations 1.1 and 1.2 can be used to calculate the number of vibrational modes for a molecule with *N* number of atoms. A vibration occurs when the bond distance (R) changes. The vibrational potential energy function between atoms *a* and *b* is shown in Equation 1.12, where *E* is the electronic energy and V_{NN} is the nuclear repulsion energy.

$$V = E + V_{NN} = E + \frac{Z_a Z_b e^2}{4\pi\varepsilon_0 R} \qquad [1.12]$$

As R decreases, the attractive forces between the atoms cause the potential energy to decrease. However, if R becomes too small, the repulsive force between electrons from each atom increases the potential energy. Therefore, there is an optimal distance between atoms in which the potential energy is a minimum. When R becomes too large, the two atoms dissociate and the potential energy plateaus. The bond dissociation energy (D_0) is the amount of energy required for dissociation from the vibrational ground state. This plateau causes the potential energy curve for a true molecule to be anharmonic, unlike the potential energy curve for the harmonic oscillator.[8] An example of a potential energy curve is shown in Figure 1.8.

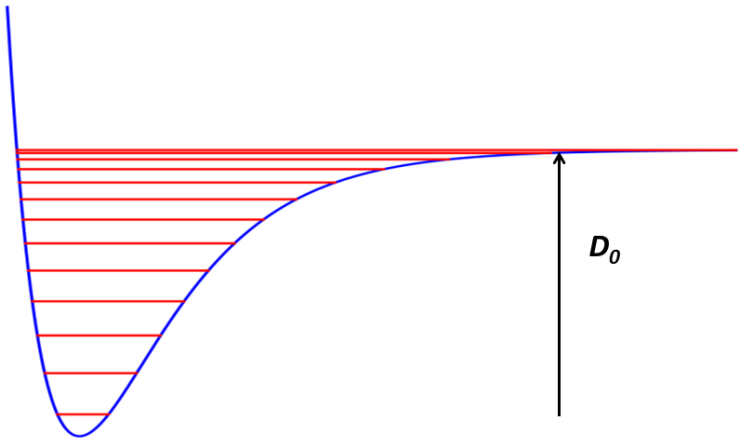

Figure 1.8. An anharmonic potential energy curve. D_0 is the dissociation energy.

A vibrating particle can be described by a set of wavefunctions $\psi_n(x)$, where n is the vibrational energy level. In order to find these wavefuctions, the Schrodinger equation for vibrational motion, shown in Equation 1.13, must be solved first.

$$-\frac{\hbar^2}{2\mu}\frac{d^2\psi_n(x)}{dx^2} + \frac{kx^2}{2}\psi_n(x) = E_n\psi_n(x) \qquad [1.13]$$

The solution to this second-order differential equation yields the normalized wavefunction in Equation 1.14, where A_n is the normalization constant.

$$\psi_n = A_n H_n(\alpha^{\frac{1}{2}} x) e^{-\alpha x^2/2} \qquad [1.14]$$

A boundary condition for the harmonic oscillator is that the amplitude of the wavefuntions remains finite as *x* increases. In order to meet this condition, the energy of each vibrational level (E_n) must follow Equation 1.15.

$$E_v = \hbar \sqrt{\frac{k}{\mu}\left(n + \frac{1}{2}\right)} = h\nu\left(n + \frac{1}{2}\right) \qquad [1.15]$$

According to Equation 1.15, the lowest vibrational state possible (v=0) still has an energy greater than zero. The frequency of oscillation (ν) is given in Equation 1.16.[9] Figure 1.9 shows an example of a harmonic oscillator.

$$\nu = \frac{1}{2\pi}\sqrt{\frac{k}{\mu}} \qquad [1.16]$$

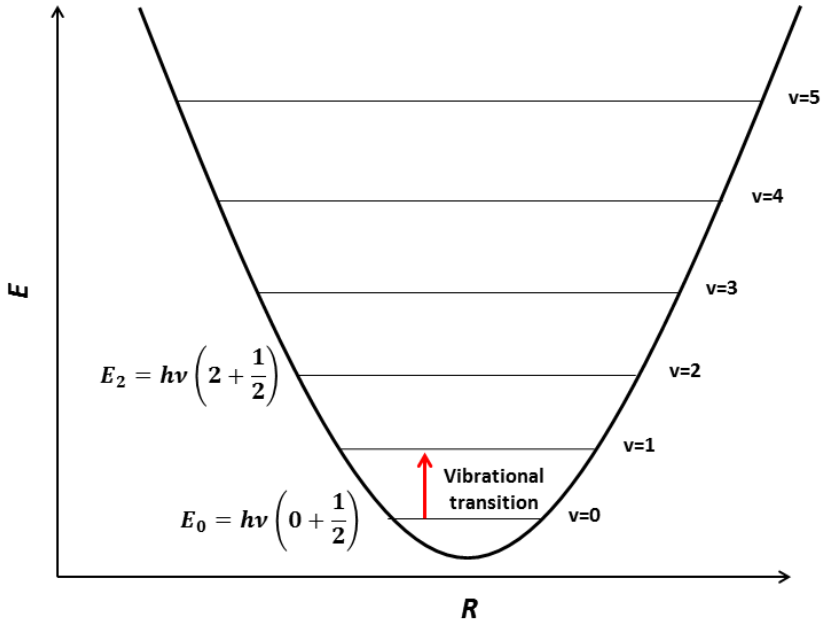

Figure 1.9. A parabolic harmonic oscillator.

1.3.3 Raman Spectroscopy

Raman spectroscopy studies a phenomenon that occurs when photons inelastically collide with a molecule. If the energy of the incident photon equals the energy of a rotational, vibrational, or electronic transition, the light will be absorbed. If the energies are not equal, the sample will scatter the light either elastically or inelastically. Elastic scattering, known as Rayleigh scattering, occurs when the energy of the scattered light equals the energy of the incident light. This normally happens when the molecule is in a vibrational ground state, is excited to a virtual state, and then relaxes back to the ground state. Inelastic scattering occurs when the energy of the scattered light does not equal the energy of the incident light. Raman scattering is a type of inelastic scattering and has two possibilities: Stokes scattering and anti-Stokes scattering. Stokes scattering occurs when a sample in its vibrational ground state is excited to a virtual state, but relaxes to an excited vibrational state. Anti-Stokes scattering occurs when a sample already in an excited vibrational state relaxes to its ground state. The different forms of scattering are shown in Figure 1.10. The differences between the ground and excited vibrational states are displayed as peaks in the Raman spectra.

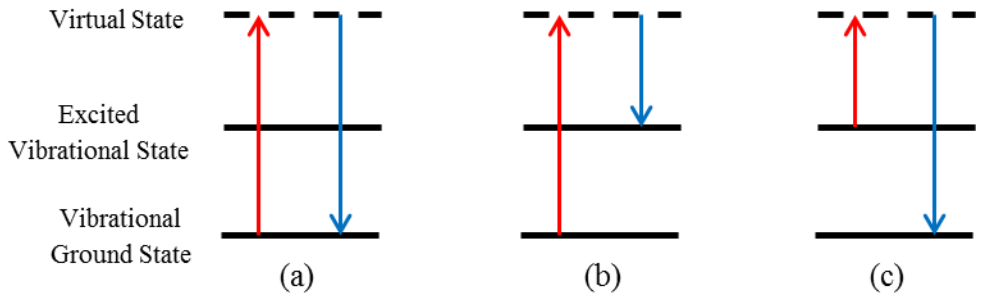

Figure 1.10. The three forms of scattering are (a) Rayleigh scattering, (b) Stokes scattering, and (c) anti-Stokes scattering.

The Raman effect can be explained in quantum mechanical terms. When a molecule with a vibrational frequency ν_{vib} is exposed to an electro-magnetic field, the molecule becomes slightly distorted. This is because the electric field causes the negatively charged electrons to shift in the opposite direction from the positively charged nucleus. This causes a time-dependent dipole moment ($\mu_{induced}(t)$) in the molecule. The dipole moment is proportional to the magnitude of the electric field according to its polarizability (α). This relationship is shown in Equation 1.17.

$$\mu_{induced}(t) = \alpha E_0 \cos(2\pi \upsilon t) \qquad [1.17]$$

The polarizability is related to the bond length $x_e + x(t)$, as shown in the Taylor-Maclaurin series in Equation 1.18.

$$\alpha(x_e + x) = \alpha(x_e) + x\left(\frac{d\alpha}{dx}\right)_{x=x_e} + \cdots \qquad [1.18]$$

The vibration of the molecule also causes time-dependent $x(t)$ to equal:

$$x(t) = x_{max} \cos(2\pi \upsilon_{vib} t) \qquad [1.19]$$

Integrating Equations 1.18 and 1.19 into Equation 1.17 yields Equation 1.20.

$$\mu_{induced}(t) = \alpha(x_e) E_0 \cos(2\pi \upsilon t) \qquad [1.20]$$
$$+ \left[\left(\frac{d\alpha}{dx}\right)_{x=x_e}\right] x_{max} E_0 [\cos\{2\pi(\upsilon + \upsilon_{vib})t\} + \cos\{2\pi(\upsilon - \upsilon_{vib})t\}]$$

According to Equation 1.20, the time-dependent dipole moment can scatter light of equal frequency as the dipole moment or at frequencies ν, (ν - ν_{vib}), and ($\nu + \nu_{vib}$). These three frequencies refer to the frequencies of Rayleigh, Stokes, and anti-Stokes scattered light.[9]

Experimental Raman spectra of aqueous and gaseous ClO_2 show its fundamental symmetric stretching mode (ν_1) at approximately 945 cm^{-1}. Some experimental spectra of gaseous ClO_2 show the bending mode (ν_3) at 452 cm^{-1}, but the coupling of the symmetric stretch with the bend and the symmetric stretch with the asymmetric stretch decreases the intensity of the bending mode and asymmetric stretching mode to the point where they are not detectable in aqueous solutions.[10] Therefore, many previous experiments have been done to characterize ClO_2 based on changes in ν_1.[11]

1.3.4 UV-Vis Spectroscopy

When comparing the energy required for transitions among energy levels, the most amount of energy is required for electronic transitions. Rotational and vibrational transitions are induced by microwave and infrared radiation, whereas electronic transitions require greater energy radiation from the visible and ultraviolet regions. UV-Vis spectroscopy is a type of absorption spectroscopy. When a molecule in its ground state is exposed to light of a wavelength, it may be promoted to an excited energy state. In order for excitation to occur, the wavelength of incident light must correspond to an energy that is identical to the energy difference between the molecule's ground and excited states. UV-Vis spectroscopy identifies the absorbance of a molecule by measuring the amount of light that is transmitted through the molecule. Beer's Law (Equation 1.21) demonstrates this relationship. Typically, an absorption spectrum shows a broad transition, called an absorption band, over a range of wavelengths instead of discrete peaks. In most molecules, excitation to more than one vibrational and/or rotational level occurs, creating a continuum of absorption.

$$\log\left(\frac{I_o}{I}\right) = A = \varepsilon bc \qquad [1.21]$$

$$\frac{I_o}{I} = transmittance$$

The type of excitation that occurs during absorption spectroscopy depends on the wavelength range of the incident light. For example, absorption of microwaves causes the sample to excite to rotational energy levels. Absorption of infrared radiation causes the sample to excite to vibrational energy levels. Absorption of ultraviolet and visible radiation causes the sample to excite to electronic energy levels as well as vibrational and rotational energy levels within the electronic excited state. Therefore, absorption spectroscopy can be used to characterize vibrational and rotational modes of excited states.

1.3.5 Comparing the Raman and UV-Vis Spectra of Chlorine Dioxide

The transition from the ground $X\,^2B_1$ state to the $A\,^2A_2$ state of ClO_2 yields an absorption band with its maximum absorbance at ~350 nm (Figure 1.11). Previous studies have constructed *ab initio* absorption spectra from potential energy surfaces in order to define the vibronic progressions within the absorption band.[12] These studies have found that the large peaks in the spectrum are formed when the symmetric stretch (ν_1) is excited to higher vibrational levels in the excited state. The vibrational level to which each mode is excited is labeled above each peak. These peaks are broadened by the coupling of the symmetric stretch and bend, as well as the coupling of the asymmetric stretch and symmetric stretch.

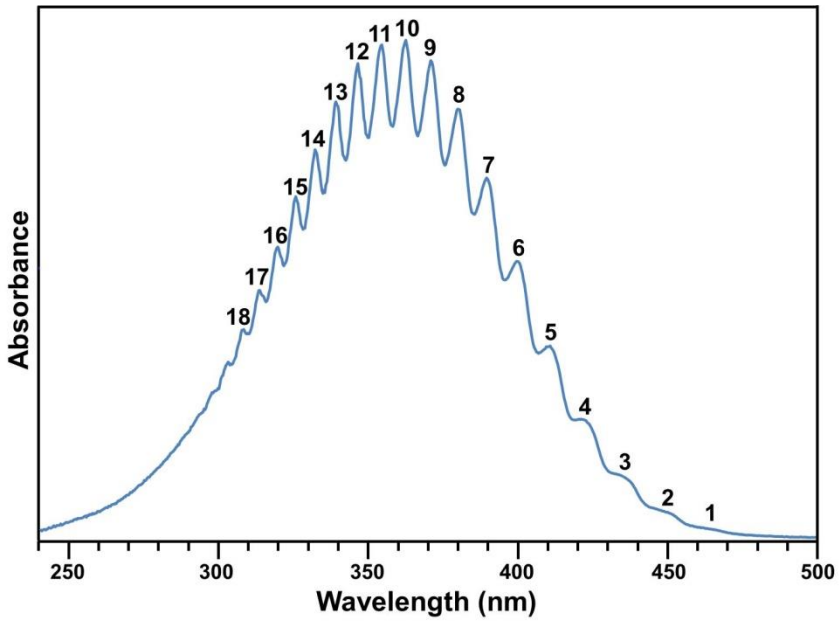

Figure 1.11. The broad band at 350 nm in the absorption spectrum of aqueous ClO_2 is the result of a transition from the ground $X\,^2B_1$ state to the $A\,^2A_2$ excited state. The discrete peaks within the broad band show the vibronic progression of ν_1 in the excited state. The number above each peak represents the vibrational level in the excited state to which ν_1 is excited.

When comparing the Raman spectrum to the absorption spectrum of ClO_2, students may initially expect the value determined for ν_1 from the absorption spectrum to be the same as that in the Raman spectrum. It is instructive to point out that Raman (or infrared absorption) spectra yield vibrational energies for the ground electronic state, whereas an absorption spectrum reports the energies of vibrational modes in excited states, as shown in Figure 1.12. Previously, ν_1 for the ground state was determined to be 945 cm^{-1} and for the *A* excited state 708.6 cm^{-1}.[5,13] The energy difference of the symmetric stretch is smaller in the excited state than the ground state.

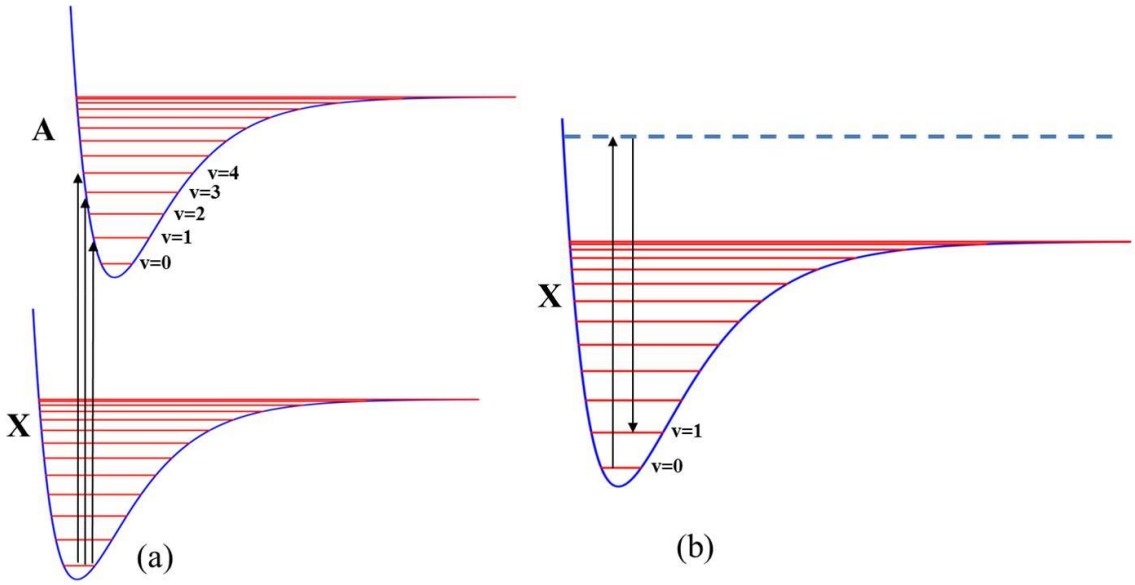

Figure 1.12. UV-Vis absorption spectroscopy and Raman spectroscopy study different energy transitions. (a) UV-Vis absorption spectroscopy studies electronic transitions. There are vibrational transitions within each electronic transition which correspond to the peaks in Figure 1.11. (b) Raman spectroscopy studies vibrational transitions.

1.4 Computational Chemistry

1.4.1 Fundamentals of Computational Chemistry

The Schrodinger equation can only be solved for one electron atoms. Numerical methods have been developed that approximate wavefunctions and values for multi-electron molecules. These methods calculate observables such as energy, bond lengths, and dipole moments. Observables are connected to the potential energy of a system through its potential energy surface (PES), which plots potential energy against the system's reaction coordinates. Transition state and equilibrium geometries of a system can be determined by finding the points on the PES in which the first derivative equals zero. For three-

dimensional systems, all partial derivatives of the PES must equal zero, as shown in Equation 1.22.

$$\frac{\delta V}{\delta R_i} = 0, i = 1,2, \ldots .3N - 6 \qquad [1.22]$$

Equilibrium geometries are characterized by a positive PES second derivative, whereas transition states are characterized by a negative PES second derivative. In a multi-dimensional system, each coordinate (R_i) yields 3N-6 second derivatives. A matrix, called a Hessian, can be constructed from these second derivatives. To determine if a given coordinate corresponds to an energy minimum, the original set of coordinates must be replaced by a new set of coordinates (ξ_i). These are referred to as normal coordinates. Stationary points in which the second derivative of the potential energy with respect to normal coordinates is positive are energy minima (Equation 1.23).

$$\frac{\delta^2 V}{\delta {\xi^2}_i} > 0 \qquad [1.23]$$

1.4.2 Hartree-Fock Orbital Theory

As stated previously, the Schrodinger equation can only be solved for one-electron systems. Therefore, approximations are made to solve the multinuclear and multi-electron Schrodinger equation shown in Equation 1.24, where E is the total energy of the system and Ψ is the wavefunction that is related to the number, identities, and positions of the electrons.

$$\hat{H}\Psi = E\Psi \qquad [1.24]$$

The equation for the Hamiltonian ($\widehat{H}$) specifies the kinetic and potential energies for each electron, as shown in Equation 1.25. Z_A is the nuclear charge of atom A, M_A is the mass of nucleus A, m_e is the mass of an electron, R_{AB} is the distance between A and B, r_{ij} is the distance between electrons i and j, r_{iA} is the distance between electron I and nucleus A, ε_0 is the premitivity of free space, and $\hbar$ is the Planck constant (h) divided by 2π.

$$\widehat{H} = -\frac{\hbar^2}{2m_e}\sum_i^{electrons}\nabla_i{}^2 - \frac{\hbar^2}{2}\sum_A^{nuclei}\frac{1}{M_A}\nabla_A{}^2 - \frac{e^2}{4\pi\varepsilon_0}\sum_i^{electrons}\sum_A^{nuclei}\frac{Z_A}{r_{iA}} + \frac{e^2}{4\pi\varepsilon_0}\sum_i^{electrons}\sum_j^{electrons}\frac{1}{r_{ij}} + \frac{e^2}{4\pi\varepsilon_0}\sum_A^{nuclei}\sum_B^{nuclei}\frac{Z_A Z_B}{R_{AB}} \quad [1.25]$$

The first approximation that is made is the Born-Oppenheimer approximation. This assumes that the nuclei in the system are stationary. Therefore, the second term in Equation 1.25, the nuclear kinetic energy, becomes zero. This yields the electronic Schrodinger equation in Equation 1.26, where the equation for the Hamiltonian is shown below.

$$\widehat{H^{el}}\Psi^{el} = E^{el}\Psi^{el} \quad [1.26]$$

$$\widehat{H} = -\frac{\hbar^2}{2m_e}\sum_i^{electrons}\nabla_i{}^2 - \frac{e^2}{4\pi\varepsilon_0}\sum_i^{electrons}\sum_A^{nuclei}\frac{Z_A}{r_{iA}} + \frac{e^2}{4\pi\varepsilon_0}\sum_i^{electrons}\sum_j^{electrons}\frac{1}{r_{ij}}$$

The electronic Schrodinger equation is still unsolvable for multi-electron systems. Therefore, the second approximation, the Hartree-Fock approximation, assumes that electrons move independently. Individual electrons are confined to spin orbitals (χ_i). An average field of (N-1) electrons is applied to each N electron individually. The multi-

electron wavefunction, or total wavefunction, Ψ is written as a determinant called the Slater determinant (Equation 1.27).

$$\Psi = \frac{1}{\sqrt{n}} \begin{vmatrix} \chi_1(1) & \chi_2(1) & \chi_n(1) \\ \chi_1(2) & \chi_2(2) & \chi_n(2) \\ \chi_1(n) & \chi_2(n) & \chi_n(n) \end{vmatrix} \quad [1.27]$$

Individual electrons are represented by each row in the detrminant. Spin orbitals are the product of molecular orbitals (ψ_i) and spin functions α or β. The existence of only two spin functions leads to the assumption that two electrons can occupy one molecular orbital. The lowest energy molecular orbitals are obtained by the self-consistent-field (SCF) procedure.

Hartree-Fock equations are differential equations that follow the Hartree-Fock approximation. These equations numerically solve for the coordinates of a single electron. An additional approximation can also be added to transform the Hartree-Fock equations into algebraic equations. This approximation assumes one-electron solutions for a multi-electron system resemble the one-electron wavefunctions for the hydrogen atom. Molecular orbitals are then described as linear combinations of a basis set of functions known as basis functions (ϕ) shown in Equation 1.28, where $c_{\mu i}$ are the molecular orbital coefficients.[9]

$$\psi_i = \sum_{\mu}^{basis\ functions} c_{\mu i}\phi_\mu \quad [1.28]$$

1.4.3 Density Functional Theory

Density functional theory (DFT) relies on the distribution of electron density of 3*N* spatial variables to solve the Schrodinger equation.[14] DFT incorporates the exact exchange-correlation functional, allowing many-body effects to be accounted for.[9,14] However, the exact exchange-correlation functional is unknown, preventing DFT methods from producing exact solutions. However, the hybrid method B3LYP includes some exact exchange, which increases its accuracy relative to full DFT methods.[14] The majority of the computations in this thesis were performed with the B3LYP method.

2 Introducing Students to a Synthetic and Spectroscopic Study of the Free Radical Chlorine Dioxide

2.1 Introduction

A primary goal of laboratory courses within science majors, including advanced inorganic, physical, or integrated chemistry courses, is for the student to gain an enhanced understanding of the material taught in lecture courses.[15] For example, the classic undergraduate physical chemistry laboratory exercise involving the absorption and emission spectra of diatomic iodine (I_2) is very popular. This popularity is largely due to the opportunity that students have to conceptually visualize molecular energy levels and directly determine molecular constants in the laboratory setting[16,17] and several variations of this lab have also been introduced.[17,18,19,20,21,22] The laboratory exercise outlined here is similar in spirit to the classic iodine lab and centers around the study of the free radical chlorine dioxide (ClO_2). ClO_2 has received a considerable amount of attention for its ability to purify drinking water without creating harmful concentrations of disinfection by-products,[1,2] its strong antimicrobial properties,[3] and its ability to oxidize atmospheric ozone.[4] It is also relatively easy to synthesize, and it has unique properties inherent to radicals that can be easily studied using optical spectroscopies and computational chemistry. Incorporating a range of concepts from multiple chemistry courses has been shown to strengthen students' ability to learn in the affective domain[23]

and a recent report on Discipline-Based Education Research from the National Research Council found that labs encompassing multiple subjects of chemistry aid in students' development of problem solving strategies.[24] Here, students synthesize aqueous ClO_2, study its physical properties using UV-Vis and Raman spectroscopies, and also have the opportunity to model its properties using computational chemistry.

As stated in the previous chapter, studies have found that the vibronic structure in the spectrum originates from the symmetric stretch (ν_1) being excited to higher vibrational energy levels. The vibrational energy level to which each mode is excited is labelled above each peak in Figure 2.1. These peaks are broadened by the coupling of the symmetric stretch and bend, as well as the coupling of the asymmetric stretch and symmetric stretch.[25]

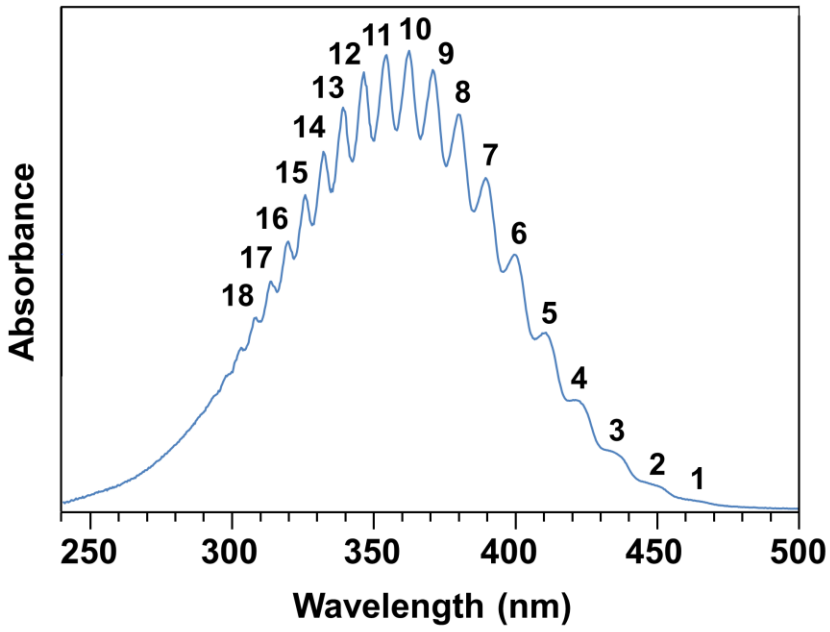

Figure 2.1. The broad band at 350 nm in the absorption spectrum of aqueous ClO_2 is the result of a transition from the ground $X\,^2B_1$ state to the $A\,^2A_2$ excited state.

For diatomic molecules, $\tilde{\nu}_e'$, the fundamental vibrational frequency, can be extrapolated from the absorption spectrum by constructing a Birge-Sponer plot.[26] The difference, in wavenumbers, between the discrete vibrational peaks in the UV-Vis spectrum ($\Delta\tilde{\nu}(v')$) is plotted against the corresponding vibrational energy level (v'). A linear fit of this graph yields a line with a slope equal to $-2\tilde{\nu}_e' x_e$ and a y-intercept equal to $\tilde{\nu}_e' - 2\tilde{\nu}_e' x_e$. The term $\tilde{\nu}_e' x_e$ corrects for anharmonicity and accounts for how rapidly the energy between the vibrational levels of the potential energy surface decreases. The fundamental symmetric stretching frequency for the *A* state of ClO_2 can also be determined in a similar fashion by plotting $\Delta\tilde{\nu}(v')$ versus v' using absorption data.

. As stated previously, it is instructive to point out that Raman (or infrared absorption) spectra yield vibrational energies for the ground electronic state, whereas an absorption spectrum reports the energies of vibrational modes in excited states (Figure 2.2). Previously, ν_1 for the ground state was determined to be 945 cm^{-1} and for the *A* excited state 708.6 cm^{-1}.[5,13] The energy difference of the symmetric stretch is smaller in the excited state than the ground state. This common occurrence can be reinforced by the optional computational chemistry component of the exercise.

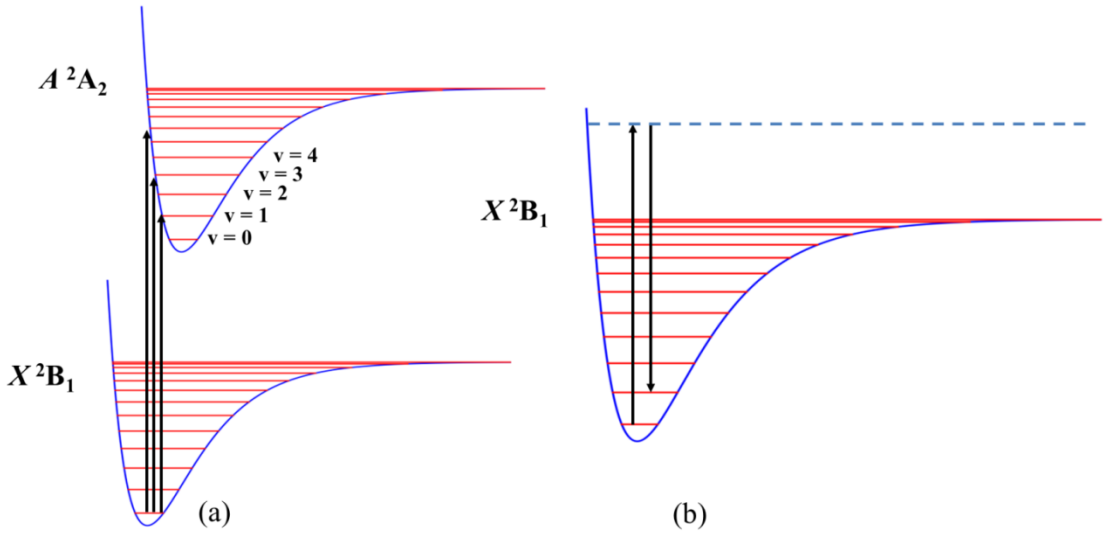

Figure 2.2. UV-Vis absorption spectroscopy and Raman spectroscopy study different energy transitions. (a) UV-Vis absorption spectroscopy studies electronic transitions. There are vibrational transitions within each electronic transition which correspond to the peaks in Figure 2.1. (b) Raman spectroscopy studies vibrational transitions.

2.2 Experimental Methods

2.2.1 Synthetic Methods

This laboratory exercise was performed by the Senior Inorganic Chemistry Laboratory Class (Chem 402) comprised of seven students at the University of Mississippi in the Spring of 2016. The chemicals used (sodium chlorite, sodium persulfate, and Ascarite) were purchased from Sigma Aldrich. The UV-Vis absorption spectrum was obtained using a Cary 100 UV-Vis spectrophotometer. The Raman spectrum was obtained with a 632 nm laser line from a Horiba Labram HR Evolution Raman Spectrometer. The computational component was executed using the Gaussian 09 software package. Both a Student Handout and Instructor Notes are included in the appendix. The Student Handout

contains background information on Raman and UV-Vis spectroscopy, the properties of ClO_2, and step-by-step experimental instructions. The Instructor Notes highlights important details to ensure a safe and efficient laboratory exercise.

The laboratory exercise was divided into three components: (1) synthesizing aqueous ClO_2, (2) obtaining both UV-Vis absorption and Raman spectra of the product, and (3) performing geometry optimizations and frequency calculations. The required synthesis and spectroscopy took approximately two and a half hours to complete. Extra time must be allotted for the computational component. This time length required for this optional component also depends on how familiar the class is with computational chemistry.

A set-up similar to the one in Figure 2.3 was first constructed. Glass tubing was hand cut prior to the lab and can be seen at locations 1, 2 and 3. The 100 mL addition funnel at location 4 was filled with an aqueous solution containing 1.579 g of sodium persulfate dissolved in 50 mL of deionized water. The 250 mL three-necked round bottom flask at location 5 contained an aqueous solution of 1.786 g of sodium chlorite dissolved in 50 mL of deionized water. The sodium persulfate solution dripped into the sodium chlorite solution at a rate of approximately 80 drops per minute. This reaction produced ClO_2 gas. The gas was bubbled out of the round bottom flask with gaseous N_2, which flowed through a rubber tube into the glass tube (or syringe, location 1) inserted into the sodium persulfate/sodium chlorite solution. The ClO_2 gas flowed from location 5 through a drying tube containing a small amount of Ascarite at location 3. Ascarite, a sodium hydroxide coated silica gel, reacted with Cl_2 gas that may have been produced during the reaction. Although the use of Ascarite is not necessary, it is highly suggested

to produce a clear UV-Vis absorption spectrum. The gas flowed through the Ascarite into the Schlenk flask (6) containing 50 mL of deionized water. The Schlenk flask was placed inside a container filled with ice. Any excess gas was trapped inside the bubbler filled with oil (7). This also prevented atmospheric gases from entering into the Schlenk flask.

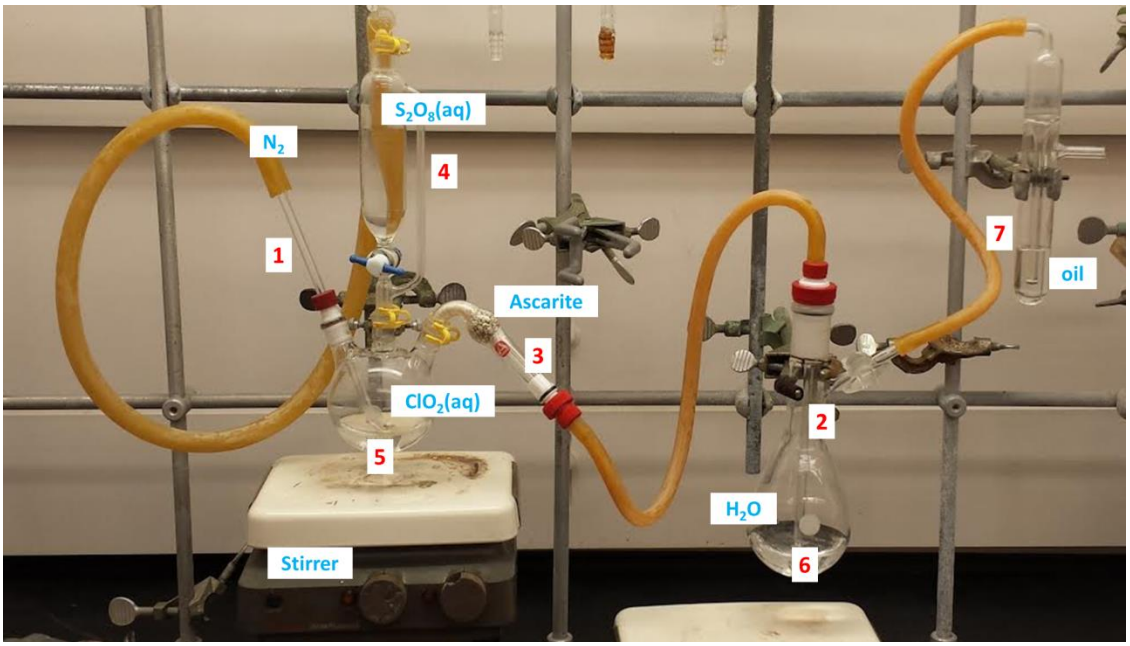

Figure 2.3. The experimental setup is shown above. The numbers indicate glassware that is referenced within the text: (1-3) glass tube, (4) addition funnel, (5) three-neck round bottom flask, (6) Schlenk flask, (7) bubbler.

The reaction proceeded for one hour. During this time, students can proceed with the optional computational chemistry component of the exercise. The solutions in the round bottom flask and Schlenk flask were a bright yellow color. A small portion of the aqueous ClO_2 solution, in the Schlenk flask, was extracted with diethyl ether. A UV-Vis spectrum of the inorganic layer, the diethyl ether extraction containing ClO_2, was obtained from 250-500 nm. Diethyl ether is used so that sharper peaks can be obtained

due to reduced hydrogen bonding between ClO_2 and water. The remaining aqueous ClO_2 was used to obtain a Raman spectrum from 500-1100 cm^{-1}.

2.2.2 Computational Methods

The optional computational chemistry component was included. For the results presented here, computations were performed with the *Gaussian 09* software package.[27] NBO calculations were performed with NBO 3.1 software[28] installed within the *Gaussian 09* software package. The structure of ClO_2 was initially drawn in *Gaussview,* with chlorine in the center bonded to oxygen on either side. Alternately, students can construct a z-matrix using C_{2v} symmetry or use the one provided in the Student Handout. This structure was optimized and its frequencies were calculated in the ground state with MP2 method and aug-cc-pVTZ basis set. A full NBO analysis of the ground state optimized geometry is also performed to calculate each atom's partial charge. The absorption spectrum of the first excited state was simulated using CIS method and the same basis set. If the number of states involved in the CIS calculation is not specified, the three lowest energy states will be calculated. Both the $X\ ^2B_1$ state and $A\ ^2A_2$ state of ClO_2 are low energy, so the number of energy states does not need to be specified in the CIS method. The frequencies of the first excited state were also calculated with CIS method and the same basis set. Sample input files are included in the student handout in the appendix.

2.2.3 Hazards

Gaseous ClO_2 is a respiratory and eye irritant. Repeated severe exposure has been shown to irritate eyes and throat, produce nasal discharge, and induce coughing. Delayed-onset pulmonary edema and chronic bronchitis could also occur. Oral consumption can decrease hemoglobin and red blood cell counts. Some studies have shown that prolonged oral consumption is associated with neurotoxicity and depression.[29] ClO_2 cannot be compressed or stored because it decomposes into chlorine and oxygen over time. At high concentrations, gaseous ClO_2 is highly explosive. A concentration of 0.1 ppm is acceptable according to the Occupational Health and Safety Administration[30] and levels here should be far below that. In this laboratory exercise, gaseous ClO_2 is formed at location 5 in Figure 2.3 and travels to location 6, where it is extracted in aqueous solution. Care must be taken, therefore, to prevent leaks and when extracting the aqueous ClO_2.

2.3 Results and Discussion

At the end of the experimental section of the lab, students should have an experimental UV-Vis spectrum, as shown in Figure 2.1, and an experimental Raman spectrum, as shown in Figure 2.4. If the computational component was completed, students should then also have a simulated UV-Vis spectrum, vibrational frequencies of the ground and excited states, and the results of the NBO analysis. Students may also generate simulated vibrational spectra by summing Lorentzian profiles as we demonstrated in this Journal earlier.[31] The experimental UV-Vis spectrum is used to create a Birge-Sponer plot, similar to the one in Figure 2.5, and determine ν_1 for the $A\ ^2A_2$ excited state. Students

should then compare this value to the value of ν_1 in the experimental Raman spectrum and be able to explain why the values are not the same. This reinforces conceptual understanding of differences between the benefits of using different spectroscopic methods and comparing ground and excited state properties of molecules using Figure 2.2.

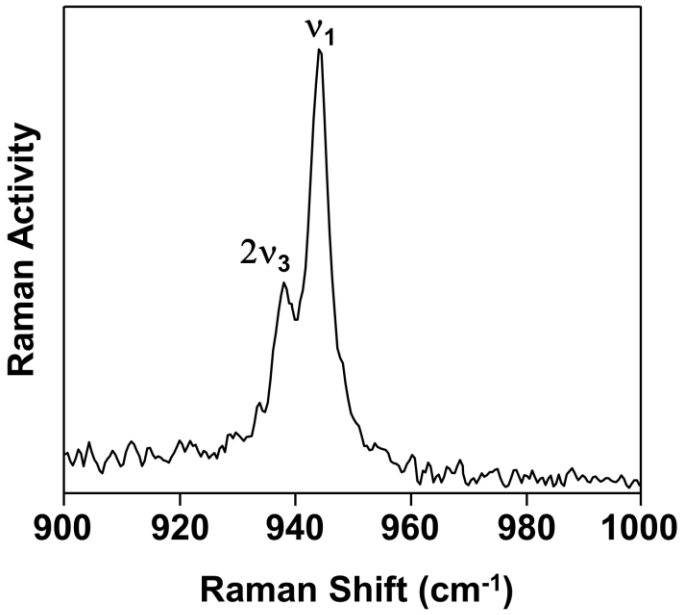

Figure 2.4. The experimental Raman spectrum, with a characteristic peak ν_1 at 945 cm^{-1}, was obtained by students.

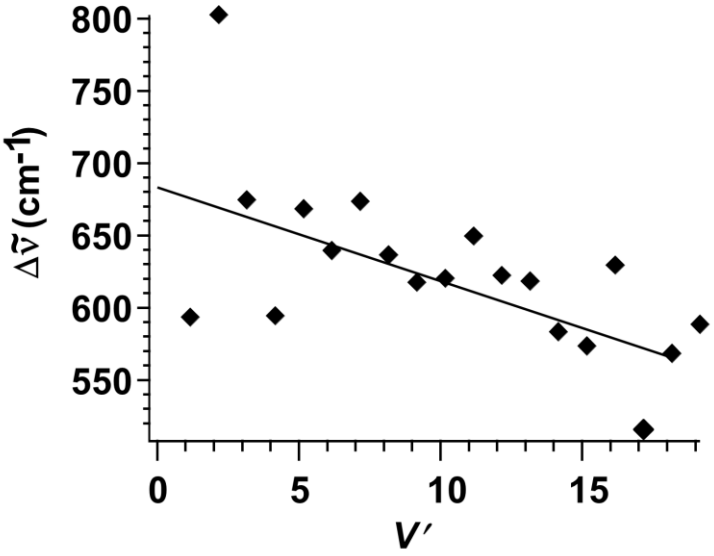

Figure 2.5. A Birge-Sponer plot constructed from an experimental UV-Vis absorbance spectrum. The value of ν_1 for ClO_2's *A* state was extrapolated from the plot to be 688 cm^{-1} in solution.

For students who complete the optional computational component of the lab, differences between the experimental and simulated spectra should be noted. The value of ν_1 determined from the Birge-Sponer plot (688 cm^{-1}) should be similar to the value of ν_1 from the computed excited state symmetric stretching frequency at the CIS/aug-cc-pVTZ level of theory (757 cm^{-1}). At the MP2/aug-cc-pVTZ level of theory, the symmetric stretch for the ground state was computed to be 1004 cm^{-1} compared to the experimental value of 945 cm^{-1} in solution. The maximum absorbance of the simulated excited state UV-Vis spectrum (475 nm) should also be relatively close to the maximum absorbance of the experimental UV-Vis spectrum (350 nm). NBO analysis should confirm that partial charges of O1 and O2 are negative while the partial charge of Cl is positive. The results of an NBO calculation are summarized in Table 2.1.

Table 2.1. The results of the NBO calculations are presented. The natural population of electrons indicates more electron density resides on O1 and O2, causing them to have negative natural partial charges. This shift in electron density causes the Cl to have a positive partial charge.

		Natural Population			
Atom	**Natural Charge**	**Core**	**Valence**	**Rydberg**	**Total**
Cl	1.23468	9.99972	5.62838	0.13722	15.76532
O1	-0.61734	1.99995	6.58103	0.03636	8.61734
O2	-0.61734	1.99995	6.58103	0.03636	8.61734
Total	**0**	**13.99962**	**18.79043**	**0.20995**	**33.00000**

Each student in the 2016 lab successfully obtained a UV-Vis and Raman spectrum and completed the computational component. Each experimental UV-Vis spectrum had a maximum absorbance approximately equal to 350 nm, and ν_1 approximately equaled 945 cm^{-1} on each Raman spectrum. Students were also able to obtain a value for ν_1 by constructing Birge-Sponer plots and were able to compare the maximum absorbance of his or her computed and experimental UV-Vis spectra. Each student also completed an assessment after the laboratory exercise was completed. The results are reported in Table 2.2.

Table 2.2. After participating in the laboratory exercise, each student ranked their agreement with each statement on a five-point scale.

	Statement for Student Response	Average Scores[a] (N=7)
1	I know what a free radical is.	4.6
2	I know what spectroscopy is.	4.6
3	I know what absorption spectroscopy is.	4.6
4	I know what energy levels are excited during absorption spectroscopy.	4.6
5	I know what Raman spectroscopy is.	4.6
6	I know what energy levels are excited during Raman spectroscopy.	4.6
7	I know what a vibrational transition is.	4.6
8	I can create a molecule in Gaussview.	4.4
9	I can run a geometry optimization calculation.	4.2
10	I can run a frequency calculation.	4.2
11	I can simulate an absorption spectrum.	4.0
12	I can simulate a Raman spectrum.	4.0
13	I know why simulated and experimental spectra are different.	4.4
14	I know why peaks are formed in spectra.	4.4

[a] Each student ranked their agreement with each statement on a five point scale with 5 indicating "Strongly Agree," 4 indicating "Agree," 3 indicating "Neither Agree nor Disagree," 2 indicating "Disagree," and 1 indicating "Strongly Disagree."

2.4 Conclusions

This advanced undergraduate laboratory exercise integrates multiple fields of chemistry, which helps students integrate the material in the affective domain.[23] Studying ClO_2 also

allows students to learn about the unique properties of free radicals along with strengthening their understanding of the uses of different forms of optical spectroscopy. The optional computational section requires students to perform difficult excited state calculations and be able to interpret differences between experiments and computations.

This work was published in the *Journal of Chemical Education* in March 2017. The reference for this work is shown below:

Introducing Students to a Synthetic and Spectroscopic Study of the Free Radical Chlorine Dioxide
Sarah C. Sutton, Walter E. Cleland, and Nathan I. Hammer
Journal of Chemical Education **Article ASAP**
DOI: 10.1021/acs.jchemed.6b00599

3 A Spectroscopic and Computational Study of ClO_2/Water Hydrogen Bonded Networks

3.1 Introduction

Chlorine dioxide (ClO_2) has been a molecule of interest over the past century due to its extreme antimicrobial properties and its role in stratospheric ozone depletion. ClO_2 is a relatively stable free radical with C_{2v} symmetry.[25,32] Much has previously been published about the molecule's potential energy surface (PES) to explain its unique absorption spectrum,[25,33,34,35] optimized ground-state geometry,[36] ionization properties,[37] and photochemistry.[38]

ClO_2 is also being used in the health industry to sterilize medical equipment. ClO_2 has demonstrated strong antimicrobial properties, being able to kill hydrogen-peroxide-resistant bacteria. Although the exact mechanism is unknown, it is theorized that ClO_2 damages the internal membrane of spores and does not interfere with its DNA.[3] ClO_2 has been proven to be effective against biological bacteria such as *Bacillus anthracis* [39,40], *Bacillus cereus, C. perfringens* [41], and *Legionella sp.*[42]

Aqueous solutions containing ClO_2 are extremely reactive oxidants. Chlorine has been traditionally used to rid drinking water and wastewater of pharmaceuticals, personal care products,[43,44,45] bacteria,[46] and other micropollutants.[45] ClO_2 solutions are becoming more desirable than chlorine-containing solutions for waste-water treatment and water

purification for several reasons. Like chlorine, ClO_2 produces minimal disinfection byproducts (DBPs) during the water purification process.[47] These chlorinated DBPs include chloroform and trihalomethanes (THMs), which have been proven to cause cancer.[2,48] In 1974, Rook discovered that chloroform and THMs had higher concentrations in water treated with chlorination methods than in raw surface water.[49] This sparked new interest in identifying other possible DBPs and developing methods to eliminate DBP production in water treatments. Summaries of chlorinated DBPs and their relative carcinogenicity and mutagenicity can be found in the literature.[50,51,52,53]

When exposed to near ultraviolet light for an extended period of time, ClO_2 photoisomerizes into its linear form. The ClOO conformation can further photodissociate into either ClO + O or Cl + O_2, shown in Equations 3.1 and 3.2. The formation of atomic chlorine (Cl) is believed to greatly contribute to ozone depletion,[38] so ClO_2 photoisomerization kinetics have been studied extensively. Although the unsymmetrical ClOO structure of chlorine dioxide is thermodynamically more favorable than the symmetrical OClO structure by 4 kcal/mol, the bond dissociation energy of ClOO is only 4.83±0.05 kcal/mol. When compared to the bond dissociation energy of OClO, 55.2±2 kcal/mol, the dissociation of ClOO is more thermodynamically favorable.[54] However, the maximum value for the quantum yield of Cl (Φ_{Cl}) is only 0.04. When ClO_2 is condensed into an aqueous solution, Φ_{Cl} increases to 0.1. The magnitude of the asymmetric stretch decreases in solution, causing ClO_2 to maintain its C_{2v} symmetry in its excited state. The conservation of C_{2v} symmetry is believed to cause the increase in Φ_{Cl} in solution.[6]

$$OClO + h\nu \rightarrow ClO + O \qquad [3.1]$$

$$OClO + h\nu \rightarrow Cl + O_2 \qquad [3.2]$$

Previous studies have shown the reaction kinetics and the photodissociation mechanism of ClO_2 to be solvent dependent.[6,55,56] However, very little is known about the solute-solvent interactions ClO_2 forms. M. P. Philpott et. al hypothesized the intermolecular ClO_2-solvent as well as solvent-solvent hydrogen bonded networks effect the photodissociation relaxation rate constants.[57] However, C. E. Foster proposed vibronic relaxation of ClO_2 to be solvent independent.[55]

This paper begins to describe ClO_2-solvent interactions by characterizing the hydrogen bonded networks ClO_2 forms with water. Water was chosen as a solvent because of the wide use of ClO_2 in water purification systems. Geometry optimization and Raman frequency calculations of $ClO_2/(H_2O)_x$(x=1-3) in the ground state were performed using the unrestricted B3LYP method and the split valence basis sets 6-31+G(*d*,*p*) and 6-311++G(*2df*,*2dp*). C. A. H. Aguilar previously used the B3LYP method with the 6-31+G(*d*,*p*) basis set to compute the optimized geometries of ClO_2 and various aniline compounds.[58] This study also focuses on changes in the fundamental symmetric stretching mode (ν_1), located at ~945 cm^{-1}, due to increased solvation. This mode was chosen because ν_1 can be observed experimentally and has been examined in previous studies.[4,11] The calculated Raman shifts for ν_1 were then compared to the experimental Raman shifts of ClO_2 solutions at various concentrations. Experimental and computed Raman spectra of ClO_2 solvated with methanol were also obtained. These were compared to the spectra of ClO_2 in water in order to determine solvent effects on hydrogen bond formation.

3.2 Experimental Methods

Gaseous ClO_2 was synthesized using the procedure outlined in Chapter 2 and dissolved in water and methanol. Samples of these ClO_2 solutions were obtained after the reaction ran for 30, 45, 60, 75, and 90 min. The chemicals used (sodium chlorite, sodium persulfate, and Ascarite) were purchased from Sigma Aldrich. The Raman spectra were obtained with a 632 nm laser line with an 1800 grating from a Horiba Labram HR Evolution Raman Spectrometer. Computations were executed using the *Gaussian 09* software package.[27] The hybrid DFT method B3LYP[59,60] was employed with the split valence basis sets 6-31G(*d,p*) and 6-311++G(*2df,2pd*). Harmonic frequency calculations confirmed the optimized geometries correspond to true local minima. Saddle point geometries of $ClO_2/(H_2O)_3$ clusters are also included in the results.

3.3 Results and Discussion

The optimized $ClO_2/(H_2O)_x$(*x*=1-3) are shown in Figures 3.1, 3.2, 3.3, and 3.4. Hydrogen bonds and van der Waals interactions appear as dotted yellow lines. These structures show the unique nature of the dipole moment of ClO_2. The partially negative O atoms form hydrogen bonds with the hydrogens of the water molecules, whereas the partially positive Cl atoms form van der Waals interactions with the oxygen of the water molecules.

The ClO_2/H_2O clusters computed with the 6-31G(*d,p*) basis set are shown in Figure 3.1. Structures 1wa and 1wb appear to be the same structure, but the position of H_2O relative to the *xz* plane of ClO_2 is different. The H_2O in 1wa lies along the *xz* plane

of ClO_2; the H_2O in 1wb is shifted along the *y*-axis of ClO_2. Structures 1wa, 1wb, and 1wc all have the same energy. Structure 1wd is slightly higher in energy by a difference of 0.286 kcal/mol. The energy of each structure and the bond energy between ClO_2 and water are outlined in Table 3.1.

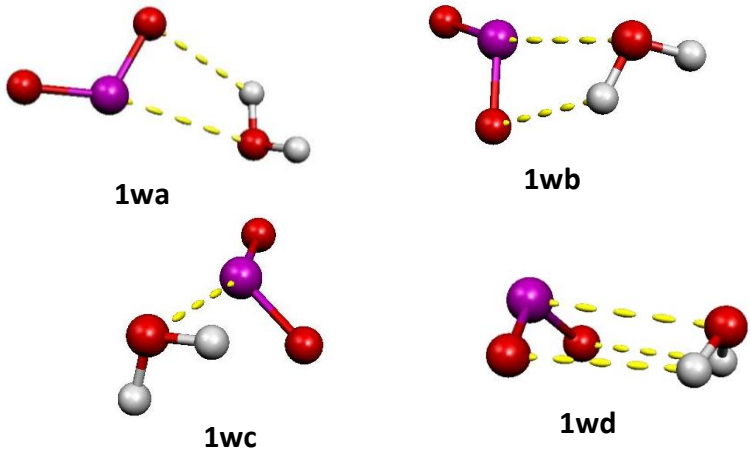

Figure 3.1. ClO_2/H_2O geometries optimized with UB3LYP/6-31G(*d*,*p*) level of theory.

Table 3.1. The energy of each structure and the energy of 1wd relative to the lower energy structures are summarized below. The bond energy between ClO_2 and water is also included.

Structure	Energy (Hartree)	Energy (kcal/mol)	Relative Energy (Hartree) to 1wa	Relative Energy (kcal/mol) to 1wa	Bond energy (kcal/mol)
1wa	-686.8461144	-4.31×10^5	0	0	-3.91
1wb	-686.8461144	-4.31×10^5	0	0	-3.91
1wc	-686.8461144	-4.31×10^5	0	0	-3.91
1wd	-686.8456593	-4.31×10^5	0.20118398	0.286	-3.26

The optimized $ClO_2/(H_2O)_2$ structures computed with the 6-31G(*d*,*p*) basis set are shown in Figure 3.2. Structures 2wb and 2wd are the lowest energy structures. The difference in each structure's energy relative to 2wb and 2wd is recorded in Table 3.2. This table also contains the bond energy between ClO_2. The bond energy for 2wb, 2wc,

2wd, and 2we are significantly lower (approximately 3 kcal/mol) than those of 2wa, 2wf, and 2wg. This could be due to the placement of the dipole-dipole interaction between the positively charged Cl in ClO_2 and the negatively charged O in H_2O. The dipole-dipole interaction for 2wb, 2wc, 2wd, and 2we is located out of the plane of the ClO_2 molecule, whereas the dipole-dipo le interaction for 2wa, 2wf, and 2wg is located along the plane of the ClO_2 molecule.

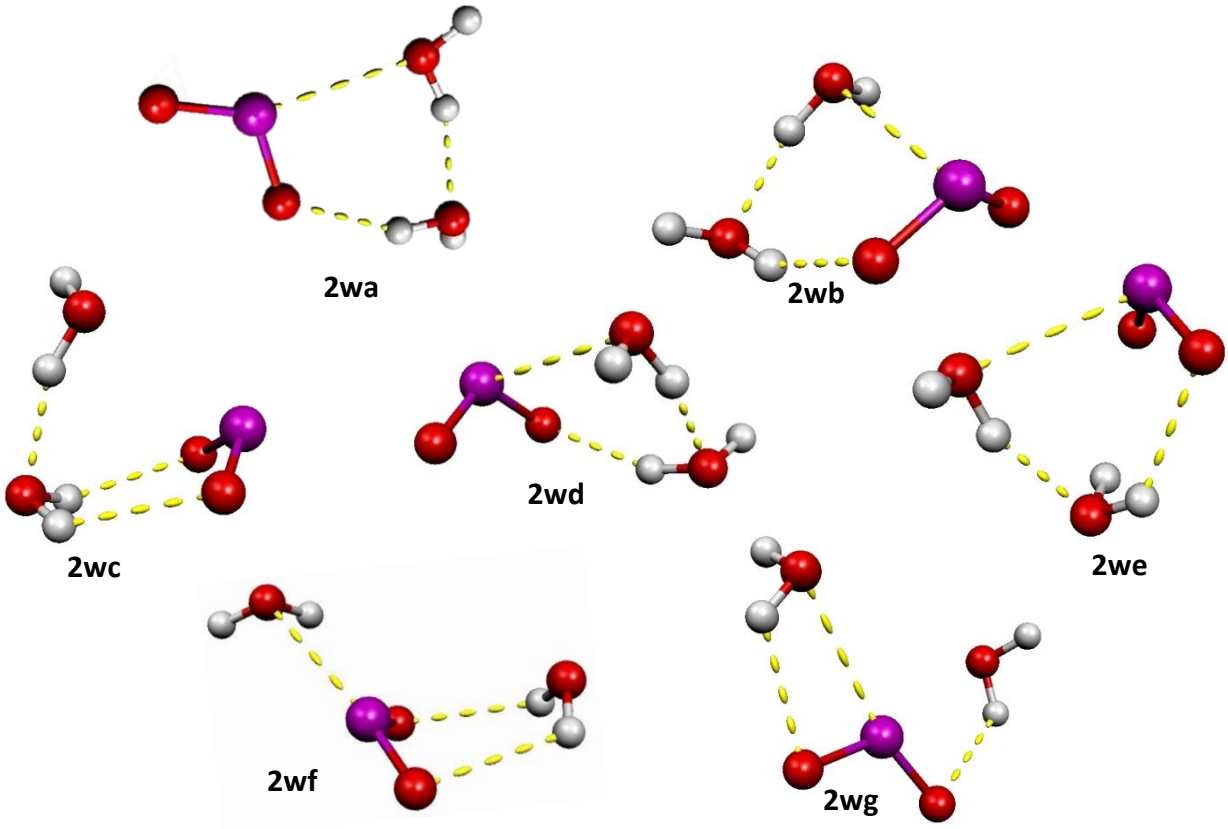

Figure 3.2. $ClO_2/(H_2O)_2$ geometries optimized with UB3LYP/6-31G(*d*,*p*) level of theory.

Table 3.2. The relative energies of each 2w structure relative to the lowest energy structures as well as the bond energy between ClO_2 and each water molecule.

Structure	Energy (Hartree)	Energy (kcal/mol)	Relative Energy (Hartree) to 2wb&2wd	Relative Energy (kcal/mol) to 2wb&2wd	Bond energy (kcal/mol)
2wa	-763.2766085	-4.78963×10^{5}	0.007359	4.61784	-6.77886
2wb	-763.2839675	-4.78968×10^{5}	0	0	-9.08778
2wc	-763.2839659	-4.78968×10^{5}	1.6×10^{-6}	1.00401×10^{-3}	-9.08727
2wd	-763.2839675	-4.78968×10^{5}	0	0	-9.08778
2we	-763.2839659	-4.78968×10^{5}	1.6×10^{-6}	1.00401×10^{-3}	-9.08727
2wf	-763.2743037	-4.78961×10^{5}	0.0096638	6.06412	-6.05572
2wg	-763.2744274	-4.78962×10^{5}	0.0095401	5.98650	-6.09453

The $ClO_2/(H_2O)_3$ structures computed with the 6-31G(*d*,*p*) basis set are shown in Figure 3.3. Structures 3wa, 3wb, and 3wj are local minima, with 3wa being the lowest energy structure. The rest of the structures are all saddle points. The energies of the three minima are shown in Table 3.3, as well as their bond energy to water and the relative energy to the lowest energy structure.

Table 3.3. The relative energies of each 3w structure relative to the lowest energy structure 3wa as well as the bond energy between ClO_2 and each water molecule.

Structure	Energy (Hartree)	Energy (kcal/mol)	Relative Energy (Hartree) to 2wa	Relative Energy (kcal/mol) to 2wa	Bond energy (kcal/mol)
3wa	-839.7522283	-5.26952×10^{5}	0	0	-16.2083
3wb	-839.7100807	-5.26926×10^{5}	0.0421476	2.64480×10	-7.3923
3wj	-839.7188478	-5.26931×10^{5}	0.0333805	2.09466×10	-9.2559

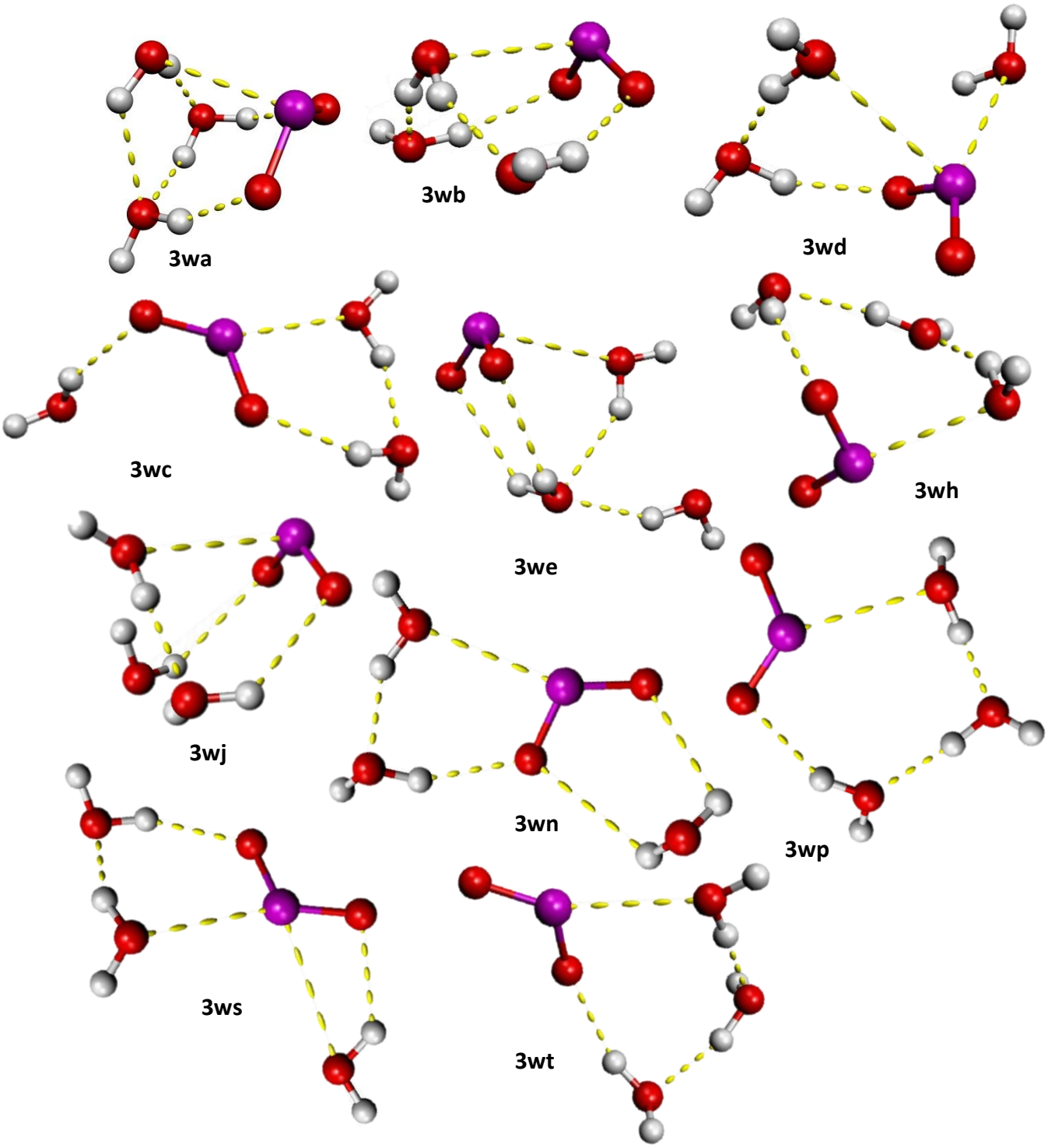

Figure 3.3. $ClO_2/(H_2O)_3$ structures optimized with UB3LYP/6-31G(*d*,*p*) level of theory.

The values for ν_1 using the 6-31G(*2df*,*2pd*) basis set differed from experimental value (945 cm^{-1}) by ~45 cm^{-1}. Computations performed with the 6-311++G(*2df*,*2pd*)

basis set yielded ν_1 values at approximately 945 cm^{-1}. The values for ν_1 are shown in Table 4. When the ClO_2/H_2O geometries were optimized with the UB3LYP/6-311++G(*2df,2pd*) level of theory, all structures converged to the 1wa structure. All $ClO_2/(H_2O)_2$ geometries also converged to the 2wa structure when optimized with the UB3LYP/6-311++G(*2df,2pd*) level of theory. This indicates the majority of the structures found with the 6-31-G(*d,p*) basis set are not true local minima. The structures 3wa and 3wb are both still local minima with the 6-311++G(*2df,2pd*) basis set, but 3wj is a saddle point.

The simulated Raman spectra of $ClO_2/(H_2O)_x$(*x*=1-3) for each *x* at the UB3LYP/6-31G(*d,p*) level of theory are shown in Figure 3.4. The lowest energy structure for each ClO_2/H_2O group was used to simulate the spectra. The simulated Raman spectra of $ClO_2/(H_2O)_x$(*x*=1-3) for each *x* at the UB3LYP/6-311++G(*2df,2pd*) level of theory are shown in Figure 3.5. The simulated spectrum for 6-31G(*d,p*) method does not show any correlation between the solvation of ClO_2 and water. The simulated spectra for the 6-311++G(*2df,2pd*) basis set shows that as ClO_2 becomes more solvated, ν_1 shifts to lower energy. This is expected because ClO_2 is able to form more hydrogen bonds as the number of water molecules present increases. When a hydrogen bond forms, charge is transferred from the hydrogen bond donor (ClO_2) to the hydrogen bond acceptor (H_2O). This decreases the mass of hydrogen bond-participating atoms, which thereby increases the bond length. The increase in bond length decreases the amount of energy required for a vibration, according to the Harmonic Oscillator equation (Equation 1.11). There is an overall red shift of 12 cm^{-1}. This is due to the increase in hydrogen bond formation as more water molecules are added. A red shift of 4 cm^{-1} is also observed in the simulated

Raman spectrum of $ClO_2/(CH_3OH)_x$(x=1,2) (Figure 3.5). However, there are no red shifts in either experimental Raman spectra (Figures 3.6 and 3.7). As the concentration of ClO_2 decreases, ν_1 is unaffected.

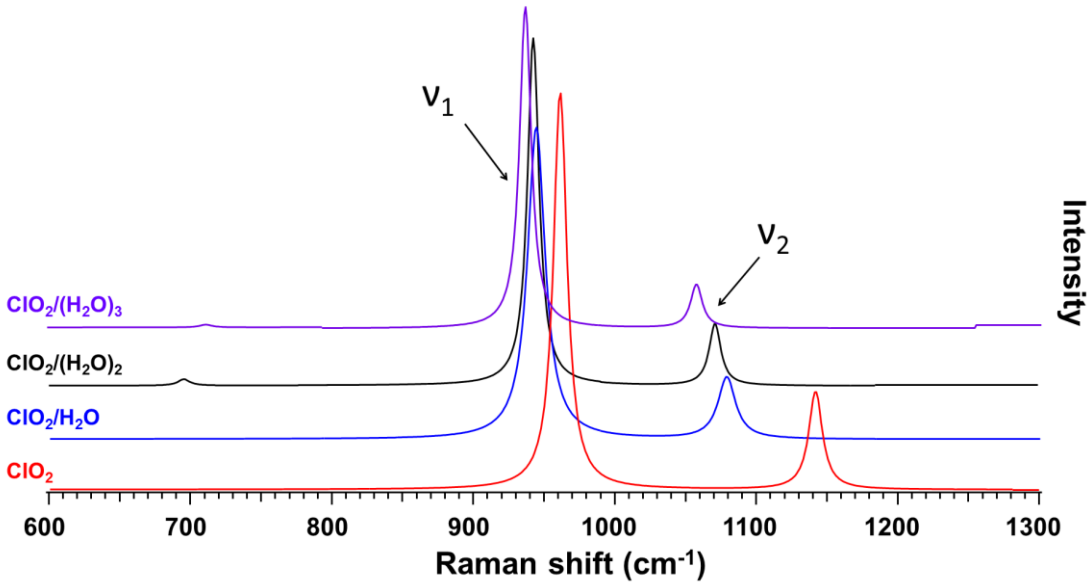

Figure 3.4. The simulated Raman spectra of $ClO_2/(H_2O)_x$(x=1-3) at UB3LYP/6-311++G(*2df,2pd*) level of theory . The spectrum of the single ClO_2 molecule is also included.

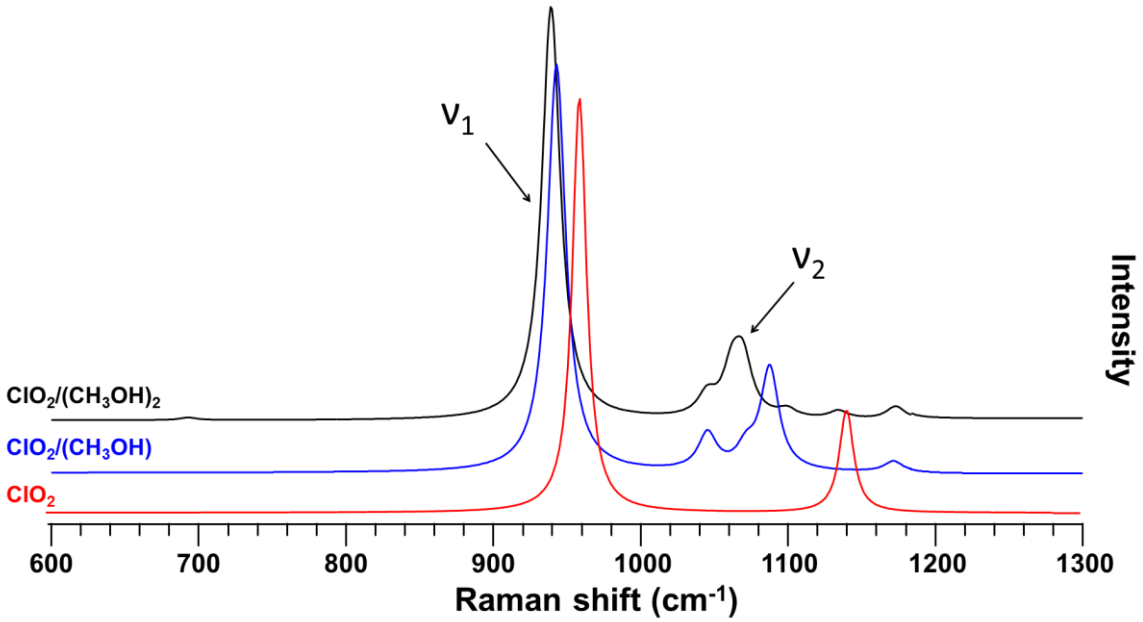

Figure 3.5. The simulated Raman spectra of $ClO_2/(CH_3OH)_x$(x=1,2) at UB3LYP/6-311++G(*2df,2pd*) level of theory. The spectrum of the single ClO_2 molecule is also included.

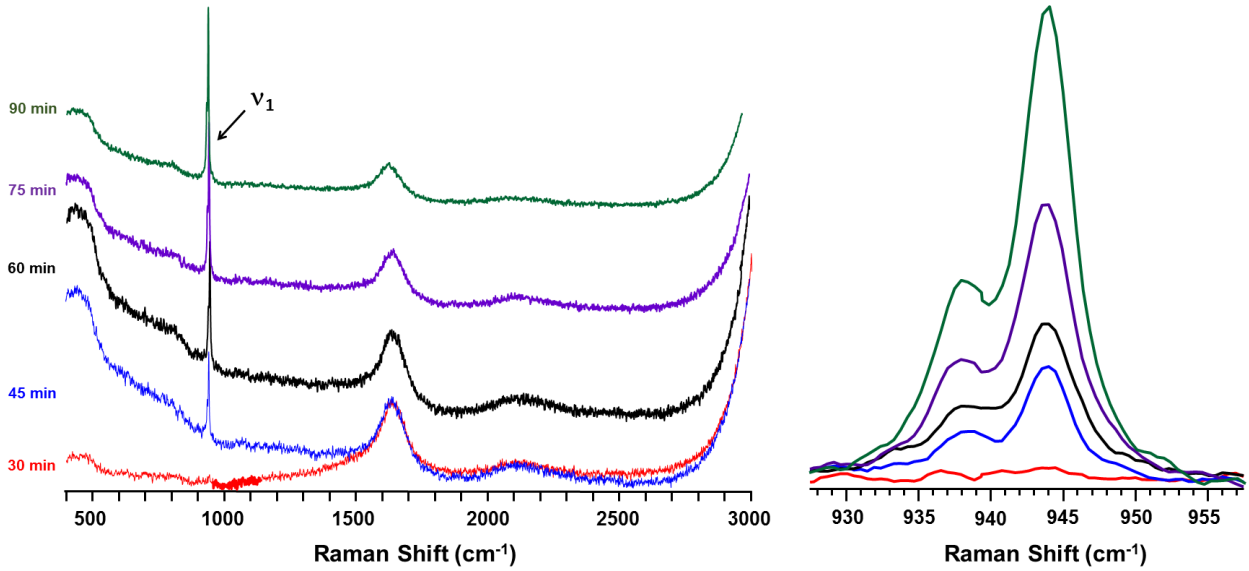

(a) (b)

Figure 3.6. (a) The experimental Raman spectrum of ClO_2 in water at increasing concentration. (b) The symmetric stretching mode (ν_1) at ~945 cm^{-1} does not shift as the concentration of ClO_2 increases.

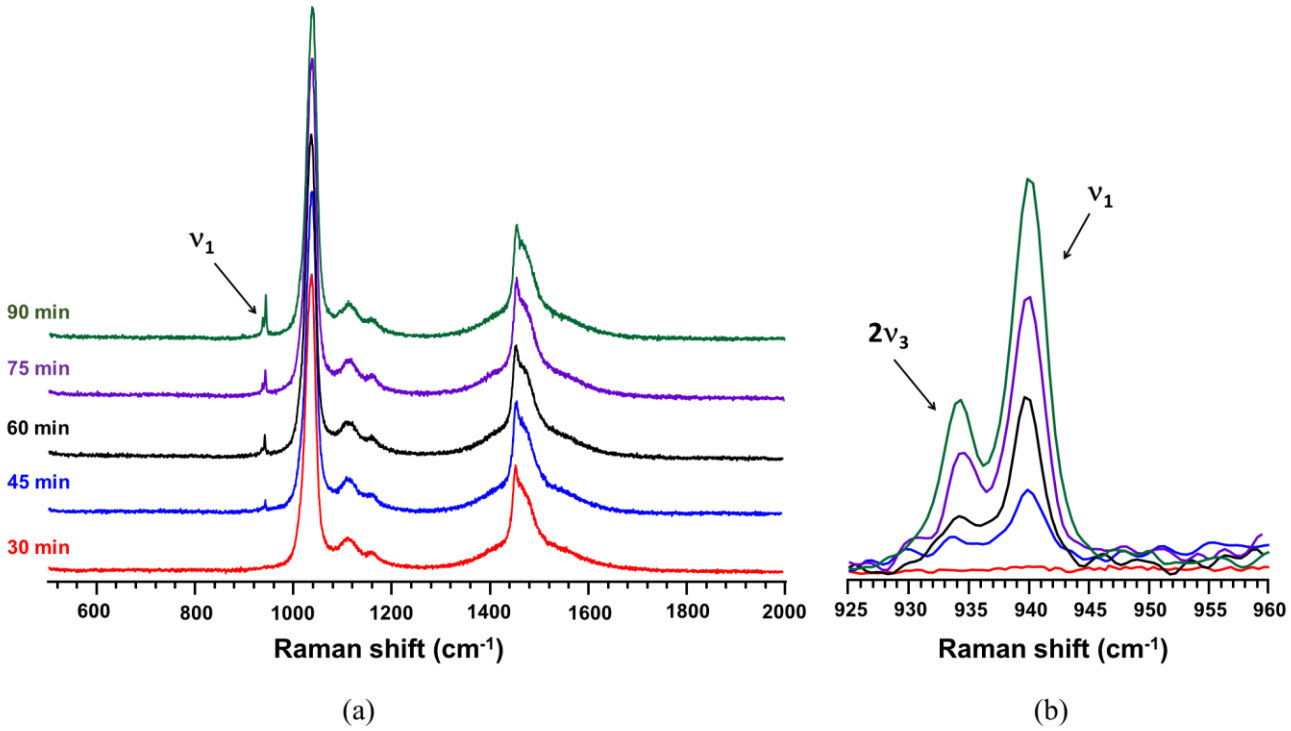

Figure 3.7. (a) The experimental Raman spectrum of ClO_2 in methanol. (b) The symmetric stretching mode (ν_1) at ~945 cm^{-1} does not shift as the concentration of ClO_2 increases.

One possible source of the discrepancy between the experimental and computed ν_1 shift could be the concentration of ClO_2 in the water and methanol solutions. For the highest concentrated solutions of ClO_2 (90 min on Figures 3.5 a and 3.6a), χ_{ClO2} only equaled 9.35×10^{-5}. For the $ClO_2/(H_2O)_3$ computations, χ_{ClO2} equally 0.25. Therefore, it is possible that the effects of hydrogen bonding, such as charge transfer and stabilization of the ground state of ClO_2, cannot be observed experimentally. However, future computational studies will add more water-ClO_2 interactions until ClO_2 is completely solvated.

When comparing the experimental Raman spectra of ClO_2 in water and methanol, ν_1 experiences a red shift of 4 cm^{-1} (Figure 3.8). This indicates stronger hydrogen bond

formation between ClO_2 and methanol than ClO_2 and water due to greater charge transfer from ClO_2 to methanol. Previous studies using resonance Raman spectroscopy have shown ν_1 red shifts in chloroform and ethanol solutions compared to water solutions.[57,61] However, no shift has been reported in the literature for ground state Raman intensities. A red shift is also observed between the computed Raman spectra of $ClO_2/(H_2O)_2$ and $ClO_2/(CH_3OH)_2$ (Figure 3.9). Table 3.4 summarizes the relative energies of the lowest energy $ClO_2/(CH_3OH)_2$ geometry optimized with the 6-311++G(*2df,2pd*) basis set and the lowest energy $ClO_2/(H_2O)_2$ geometry optimized with the same basis set. The table also compares values

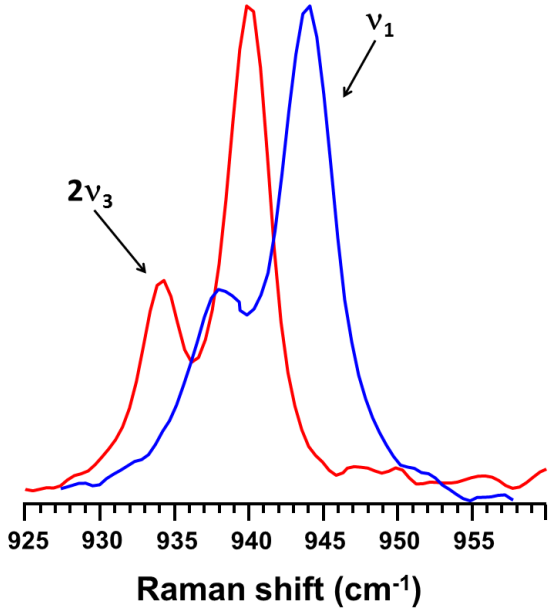

Figure 3.8. The experimental Raman spectra of ClO_2 in water (blue) and methanol (red) yield different Raman shifts for its symmetric stretching mode (ν_1). For the ClO_2/water solution, ν_1 is 944 cm^{-1}. For the ClO_2/methanol solution, ν_1 is 940 cm^{-1}.

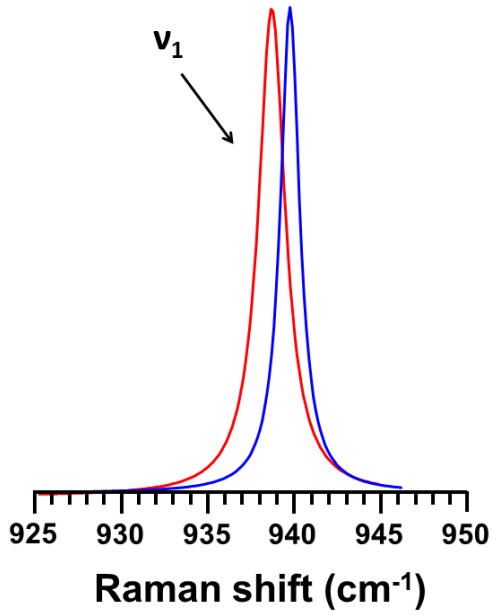

Figure 3.9. The simulated Raman spectra of ClO_2 in water (blue) and methanol (red) yield different Raman shifts for its symmetric stretching mode (ν_1). For the $ClO_2/(H_2O)_2$ structure, ν_1 is 940.96 cm^{-1}. For the $ClO_2/(CH_3OH)_2$ structure, ν_1 is 939.34 cm^{-1}.

Table 3.4. The relative energies of the structures used to construct the simulated the Raman spectra in Figure 3.9 as well as the computed and experimental values for ν_1.

Structure	Energy (Hartree)	Energy (kcal/mol)	Bond energy (kcal/mol)	ν_1 (cm^{-1})
$ClO_2/(H_2O)_2$	-763.2766085	-4.78963×10^5	-6.77886	940.96
$ClO_2/(CH_3OH)_2$	-842.104275	-5.28428×10^5	-11.36029743	939.34
Experimental ClO_2/H_2O	-	-	-	944
Experimental ClO_2/CH_3OH	-	-	-	940

3.4 Conclusions

Previous studies have attempted to explain the solvent-dependent properties of ClO_2.[6,55,56,57] The role hydrogen bonding plays in these properties has been debated in

the literature. This study began to characterize the hydrogen bonded networks ClO_2 forms with water and the effects of hydrogen bonding on the symmetric stretching mode (ν_1) on ClO_2. Overall, as the number of interactions between ClO_2 and water increased, the overall relative energy of ClO_2 decreased. This was also apparent in the red shift of ν_1 in the simulated Raman spectra. However, this red shift was not observed in the experimental Raman spectra of aqueous ClO_2. This is believed to be the result of the large difference in χ_{ClO2} between the experimental and computed ClO_2 systems. Future computational studies will add more water-ClO_2 interactions until ClO_2 is completely solvated. The experimental Raman shift for ν_1 in methanol (940 cm^{-1}) was lower in energy than the experimental Raman shift for ν_1 in water (944 cm^{-1}). This indicates stronger hydrogen bond formation between ClO_2 and methanol than ClO_2 and water. Computed Raman intensities for $ClO_2/(CH_3OH)_2$ are also lower in energy than those computed for $ClO_2/(H_2O)_2$ by 1.62 cm^{-1}. Future studies will also examine the effects of solvation on the second asymmetric stretch overtone.

This work will be submitted to the *Journal of Physical Chemistry A* in the near future.

4 References

1. Deshwal, B. R. and H. K. Lee. Manufacture of chlorine dioxide from sodium chlorate: State of the art. *Journal of Industrial and Engineering Chemistry*. **2005**, *113*, 330-346.

2. Wang, Y., H. Liu, et al. Oxidative removal of diclofenac by chlorine dioxide: Reaction kinetics and mechanism. *Chemical Engineering Journal*. **2015**, *279*, 409-415.

3. Friedline, A., M. Zachariah, et al. Sterilization of hydrogen peroxide resistant bacterial spores with stabilized chlorine dioxide. *AMB Express*. **2015**, *51*, 1-6.

4. Galashev, A. Y. The influence of atmospheric water clusters and halogen ions on ozone depletion. *Energy, Environment and Economics Research Compendium*. **2013**, 279-299.

5. Tanaka, K. and T. Tanaka. CO_2 and N_2O laser Stark spectroscopy of the n_1 band of the ClO_2 radical. *Journal of Molecular Spectroscopy*. **1983**, *982*, 425-452.

6. Brooksby, C., O. V. Prezhdo, et al. Molecular dynamics study of aqueous solvation dynamics following OClO photoexcitation. *Journal of Chemical Physics*. **2003**, *11810*, 4563-4572.

7. McHale, J. L. Molecular spectroscopy, Pearson College Division.**1999**.

8. Engel, T., P. Reid, et al. *Physical chemistry*. Boston, Pearson. **2013.**

9. Esposito, A. P., T. Stedl, et al. Absorption and Resonance Raman Study of the $^2B_1(X)-^2A_2(A)$ Transition of Chlorine Dioxide in the Gas Phase. *Journal of Physical Chemistry A*. **1999**, *10312*, 1748-1757.

10. Reid, P. J. Understanding the phase-dependent reactivity of chlorine dioxide using resonance Raman spectroscopy. *Accounts of Chemical Research*. **2001**, *349*, 691-698.

11. Sun, Z., N. Lou, et al. A $^2A_2 \leftarrow X\ ^2B_1$ absorption and Raman spectra of the OClO molecule: A three-dimensional time-dependent wave packet study. *Journal of Chemical Physics*. **2005**, *1225*.

12. Richard, E. C. and V. Vaida. The direct near ultraviolet absorption spectrum of the $\tilde{A}\ ^2A_2 \leftarrow \tilde{X}\ ^2B_1$ transition of jet-cooled chlorine dioxide. *Journal of Chemical Physics*. **1991**, *941*, 153-162.

13. Zhang, I. Y., J. Wu, et al. Extending the reliability and applicability of B3LYP. *Chemical Communications*. **2010**, *4618*, 3057-3070.

14. Hofstein, A. and R. Mamlok-Naaman. The laboratory in science education: The state of the art. *Chemistry Education Research and Practice*. **2007**, *82*, 105-107.

15. Williamson, J. C. Teaching the rovibronic spectroscopy of molecular iodine. *Journal of Chemical Education*. **2007**, *848*, 1355-1359.

16. Pursell, C. J. and L. Doezema. The electronic absorption spectrum of molecular iodine: A new fitting procedure for the physical chemistry laboratory. *Journal of Chemical Education*. **1999**, *766*, 839-841.

17. Hollenberg, J. L. Resource papers - VIII. Energy states of molecules. *Journal of Chemical Education*. **1970**, *471*, 2-14.

18. O'Brien, L. C. and R. L. Kubicek. Binding-energy curve for iodine using laser spectroscopy. *Journal of Chemical Education*. **1996**, *731*, 86-87.

19. Muenter, J. S. The Helium-Neon Laser-Induced Fluorescence Spectrum of Molecular Iodine: An Undergraduate Laboratory Experiment. *Journal of Chemical Education*. **1996**, *736*, 576.

20. Pursell, C. J. and L. Doezema. The Electronic Absorption Spectrum of Molecular Iodine: A New Fitting Procedure for the Physical Chemistry Laboratory. *Journal of Chemical Education*. **1999**, *766*, 839.

21. Lessinger, L. Morse Oscillators, Birge-Sponer Extrapolation, and the Electronic Absorption Spectrum of I2. *Journal of Chemical Education*. **1994**, *715*, 388.

22. Galloway, K. R. and S. L. Bretz. Measuring Meaningful Learning in the Undergraduate Chemistry Laboratory: A National, Cross-Sectional Study. *Journal of Chemical Education*. **2015**, *9212*, 2006-2018.

23. Singer, S. and K. A. Smith. Discipline-Based Education Research: Understanding and Improving Learning in Undergraduate Science and Engineering. *Journal of Engineering Education*. **2013**, *1024*, 468-471.

24. Sun, Z., N. Lou, et al. A 2A 2←X 2B 1 absorption and Raman spectra of the OClO molecule: A three-dimensional time-dependent wave packet study. *Journal of Chemical Physics*. **2005**, *1225*.

25. Herzberg, G. *Spectra of Diatomic Molecules*. New York, Van Nostrand Reinhold. **1950.**

26. Frisch, M. J., G. W. Trucks, et al. Gaussian 09. Wallingford, CT, USA, Gaussian, Inc.**2009**.

27. Glendening, E. D., A. E. Reed, et al. NBO Version 3.1.

28. Proctor, N. H., J. P. Hughes, et al. *Proctor and Hughes' chemical hazards of the workplace*, John Wiley & Sons. **2004.**

29. Jin, R.-y., S.-q. Hu, et al. Concentration-dependence of the explosion characteristics of chlorine dioxide gas. *Journal of Hazardous Materials*. **2009**, *1662–3*, 842-847.

30. Scardino, D. J., A. A. Howard, et al. Raman Spectroscopy as the Method of Detection for Constructing a Binary Liquid–Vapor Phase Diagram. *Journal of Chemical Education*. **2011**, *888*, 1162-1165.

31. Esposito, A. P., T. Stedl, et al. Absorption and Resonance Raman Study of the 2B1(X)−2A2(A) Transition of Chlorine Dioxide in the Gas Phase. *The Journal of Physical Chemistry A*. **1999**, *10312*, 1748-1757.

32. Xie, D. and H. Guo. A refined near-equilibrium potential energy surface and the absorption spectrum of OClO(Ã 2A2). *Chemical Physics Letters*. **1999**, *3071-2*, 109-116.

33. Duehr, O., H. Fidder, et al. Ultrafast dynamics of chlorine dioxide in solution upon excitation of the A2A2←X2B1 transition. *IQEC, International Quantum Electronics Conference Proceedings*. **1999**, 77.

34. Peterson, K. A. and H. J. Werner. Multireference configuration interaction calculations of the low-lying electronic states of ClO2. *The Journal of Chemical Physics*. **1992**, *9612*, 8948-8961.

35. Teixeira, O. B. M., V. C. Mota, et al. Single-sheeted double many-body expansion potential energy surface for ground-state ClO2. *Journal of Physical Chemistry A*. **2014**, *11826*, 4851-4862.

36. Wei, Z. Z., B. T. Li, et al. A theoretical investigation of the excited states of OClO radical, cation, and anion using the CASSCF/CASPT2 method. *Journal of Computational Chemistry*. **2007**, *282*, 467-477.

37. Thomsen, C. L., P. J. Reid, et al. Quantum yield for ClOO formation following photolysis of aqueous OClO. *Journal of the American Chemical Society*. **2000**, *12251*, 12795-12801.

38. Riesenman, P. J. and W. L. Nicholson. Role of the spore coat layers in Bacillus subtilis spore resistance to hydrogen peroxide, artificial UV-C, UV-B, and solar UV radiation. *Applied and Environmental Microbiology*. **2000**, *662*, 620-626.

39. Buhr, T. L., A. A. Young, et al. Decontamination of a hard surface contaminated with Bacillus anthracis Sterne and B. anthracis Ames spores using electrochemically generated liquid-phase chlorine dioxide (e ClO_2). *Journal of Applied Microbiology*. **2011**, *1115*, 1057-1064.

40. Foegeding, P. M., V. Hemstapat, et al. Chlorine dioxide inactivation of Bacillus and Ciosfridium spores. *Journal of Food Science*. **1986**, *511*, 197-201.

41. Kim, B. R., J. E. Anderson, et al. Literature review - Efficacy of various disinfectants against Legionella in water systems. *Water Research*. **2002**, *3618*, 4433-4444.

42. Cai, M. Q., L. Q. Zhang, et al. Influencing factors and degradation behavior of propyphenazone and aminopyrine by free chlorine oxidation. *Chemical Engineering Journal*. **2014**, *244*, 188-194.

43. Gibs, J., P. E. Stackelberg, et al. Persistence of pharmaceuticals and other organic compounds in chlorinated drinking water as a function of time. *Science of The Total Environment*. **2007**, *3731*, 240-249.

44. Lee, Y. and U. von Gunten. Oxidative transformation of micropollutants during municipal wastewater treatment: Comparison of kinetic aspects of selective (chlorine, chlorine dioxide, ferrateVI, and ozone) and non-selective oxidants (hydroxyl radical). *Water Research*. **2010**, *442*, 555-566.

45. Barbeau, B., R. Desjardins, et al. Impacts of water quality on chlorine and chlorine dioxide efficacy in natural waters. *Water Research*. **2005**, *3910*, 2024-2033.

46. Pan, Y., W. Li, et al. Formation and occurrence of new polar iodinated disinfection byproducts in drinking water. *Chemosphere*. **2016**, *144*, 2312-2320.

47. Hrudey, S. E. Chlorination disinfection by-products, public health risk tradeoffs and me. *Water Research*. **2009**, *438*, 2057-2092.

48. Rook, J. J. Uproar about chlorine [4]. *Environmental Science and Technology*. **1975**, *92*, 92-93.

49. Richardson, S. D., M. J. Plewa, et al. Occurrence, genotoxicity, and carcinogenicity of regulated and emerging disinfection by-products in drinking water: A review and roadmap for research. *Mutation Research - Reviews in Mutation Research*. **2007**, *6361-3*, 178-242.

50. Wu, M., J. Liu, et al. Effects and kinetics of chlorine dioxide for removal of Benzo[a]pyrene in water. *Environmental Engineering Science*. **2012**, *292*, 133-138.

51. Hrudey, S. E. Chlorination disinfection by-products, public health risk tradeoffs and me. *Water Res.* **2009**, *438*, 2057-2092.

52. Aieta, E. M. and J. D. Berg. A Review of Chlorine Dioxide in Drinking Water Treatment. *Journal (American Water Works Association)*. **1986**, *786*, 62-72.

53. Mahapatra, S. and G. M. Krishnan. Photoelectron spectroscopy of chlorine dioxide and its negative ion: A quantum dynamical study. *Journal of Chemical Physics*. **2001**, *11515*, 6951-6960.

54. Foster, C. E., B. P. Barham, et al. Resonance Raman intensity analysis of chlorine dioxide dissolved in chloroform: The role of nonpolar solvation. *Journal of Chemical Physics*. **2001**, *11419*, 8492-8504.

55. Chorny, I., J. Vieceli, et al. Molecular dynamics study of the vibrational relaxation of OClO in bulk liquids. *Journal of Chemical Physics*. **2002**, *11620*, 8904-8911.

56. Philpott, M. P., S. C. Hayes, et al. Intermolecular hydrogen bonding in chlorine dioxide photochemistry: A time-resolved resonance Raman study. *Chemical Physics*. **2001**, *2632–3*, 389-400.

57. Aguilar, C. A. H., J. Narayanan, et al. Kinetics and mechanism for the oxidation of anilines by ClO2: a combined experimental and computational study. *Journal of Physical Organic Chemistry*. **2014**, *275*, 440-449.

58. Becke, A. D. Density-functional thermochemistry. III. The role of exact exchange. *The Journal of Chemical Physics*. **1993**, *987*, 5648-5652.

59. Hybrid exchange-correlation functional determined from thermochemical data and ab initio potentials. *The Journal of Chemical Physics*. **2001**, *11520*, 9233-9242.

APPENDIX

A Spectroscopic Study of the Free Radical Chlorine Dioxide: Student Handout

This laboratory focuses on both the synthesis and spectroscopic analysis of the free radical chlorine dioxide (ClO_2). Students first synthesize chlorine dioxide and then analyze its symmetric stretch in both the ground and excited states using Raman and UV-Visible spectroscopies. An optional component includes exploring ClO_2's charge separation and modeling its vibrational frequencies and absorption spectrum using computational chemistry.

Learning Objectives:

(1) Apply techniques for synthesizing inorganic molecules.
(2) Describe the properties of molecular radicals.
(3) Analyze a synthetic product using molecular spectroscopy.
(4) Interpret spectroscopic data to characterize vibrational and electronic energy levels.
(5) Model physical properties using computational chemistry. (optional)

Chlorine Dioxide

Chlorine dioxide (ClO_2) is a neutral free radical with C_{2v} symmetry that acts as an oxidizing agent. ClO_2 has received a considerable amount attention for its ability to purify drinking water without creating harmful concentrations of disinfection by-products,[1,2] its strong antimicrobial properties,[3] and its ability to oxidize atmospheric ozone.[4] ClO_2's unique oxidation properties are believed to be a result of the highly selective nature of one electron-transfer reactions. In its ground state, although the unpaired electron is shared among all three atoms of ClO_2, most of the electron density resides mostly on either oxygen atom. The electronegativity of the two oxygen atoms is great enough to withdraw electron density from the chlorine atom, thereby giving chlorine an induced partial positive charge. The overall dipole moment of ClO_2 is 1.792 Debye[5] and ClO_2 has a bent molecular geometry, with a bond angle of 117.6˚. In nature, ClO_2 exists as a yellow gas that can be condensed down into a reddish-brown liquid at 11˚C and solidified to an orange-brown solid at -59˚C. Gaseous ClO_2 is highly soluble in aqueous solutions, remaining unhydrolyzed in its free radical form in the pH range from 2 to 10.[1]

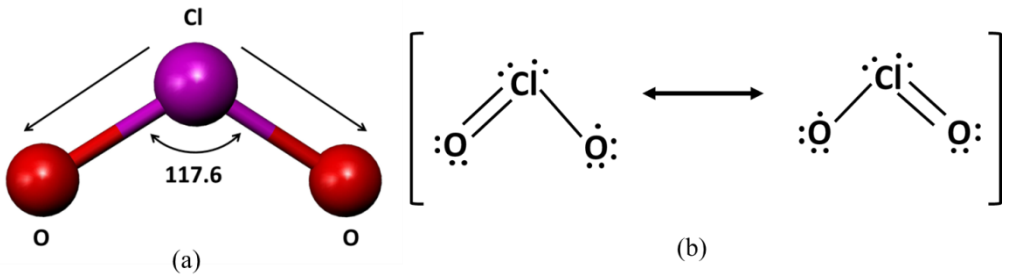

Figure 1. (a) ClO_2 has a bent conformation. The straight arrows indicate the direction in which the bonds elongate during the symmetric stretch. (b) ClO_2 has an unpaired electron that is shared among all three atoms in two different resonance structures. The unpaired electron mainly resides on one of the oxygen atoms.

Aqueous solutions containing ClO_2 are extremely reactive oxidants. ClO_2 solutions are becoming more desirable than chlorine-containing solutions for waste-water treatment and water purification for several reasons. ClO_2 oxidizes its target instead of chlorinating it, preventing the formation of harmful chlorinated organic compounds.[1] These chlorinated disinfection by-products (DBPs) include chloroform and trihalomethanes (THMs), which have been proven to cause cancer.[2,48] In 1974, Rook discovered that chloroform and THMs had higher concentrations in water treated via chlorination methods than in raw surface water.[49] This sparked new interest in identifying other possible DBPs and developing methods to eliminate DBP production in water treatments. Summaries of chlorinated DBPs and their relative carcinogenicity and mutagenicity can be found.[50]

ClO_2 is also being used in the health industry to sterilize medical equipment. ClO_2 has demonstrated strong antimicrobial properties, being able to kill hydrogen-peroxide-resistant bacteria. Although the exact mechanism of bacteria spore killing via ClO_2 is unknown, it is theorized that ClO_2 damages the internal membrane of spores and does not interfere with is DNA.[3] ClO_2 has been proven to be effective against biological bacteria such as *Bacillus anthracis* [39,40], *Bacillus cereus, C. perfringens* [41], and *Legionella sp*.[42]

When exposed to near ultraviolet light for an extended period of time, ClO_2 photoisomerizes into its linear form. The ClOO conformation can further photodissociate into either ClO + O or Cl + O_2, shown in Equation 1. The formation of atomic chlorine (Cl) is believed to greatly contribute to ozone depletion,[38] so ClO_2 photoisomerization kinetics have been studied extensively. Although the unsymmetrical ClOO structure of chlorine dioxide is thermodynamically more favorable than the symmetrical OClO structure by 4 kcal/mol, the bond dissociation energy of ClOO is only 4.83±0.05 kcal/mol. When compared to the bond dissociation energy of OClO, 55.2±2 kcal/mol, the dissociation of ClOO is more thermodynamically favorable.[54] However, the maximum value for the quantum yield of Cl (Φ_{Cl}) is only 0.04. When ClO_2 is condensed into an aqueous solution, Φ_{Cl} increases to 0.1. The magnitude of the asymmetric stretch

decreases in solution, causing ClO_2 to maintain its C_{2v} symmetry in its excited state. The conservation of C_{2v} symmetry is believed to cause the increase in Φ_{Cl} in solution.[6]

a. $OClO + h\nu \rightarrow ClO + O$
b. $OClO + h\nu \rightarrow Cl + O_2$

Equation 1. ClO_2 yields either ClO+O or Cl+O_2 when excited by near-UV light. This reaction proceeds through the intermediate ClOO, which is an isomerized form of ClO_2.

Absorption Spectroscopy

UV-vis spectroscopy is a type of absorption spectroscopy. When a molecule in its ground state is exposed to light of a wavelength, it may be promoted to an excited energy state. In order for excitation to occur, the wavelength of incident light must correspond to an energy that is identical to the energy difference between the molecule's ground and excited states. UV-vis spectroscopy identifies the absorbance of a molecule by measuring the amount of light that is transmitted through the molecule. Beer's Law (Equation 2) demonstrates this relationship. Typically, an absorption spectrum shows a broad transition, called an absorption band, over a range of wavelengths instead of discrete peaks. In most molecules, excitation to more than one vibrational and/or rotational level occurs, creating a continuum of absorption.

$$\log\left(\frac{I_o}{I}\right) = A = \varepsilon bc$$

$$\frac{I_o}{I} = transmittance$$

Equation 2. Beer's Law shows that each molecule has a characteristic absorbance, dependent on its extinction coefficient and the concentration of the sample. I_o is the intensity of incident light, I is the intensity of transmitted light, ε is the molar extinction coefficient, b is the path length (in cm), and c is the concentration of the sample (in mol/L).

The type of excitation that occurs during absorption spectroscopy depends on the wavelength range of the incident light. For example, absorption of microwaves causes the sample to excite to rotational energy levels. Absorption of infrared radiation causes the sample to excite to vibrational energy levels. Absorption of ultraviolet and visible radiation causes the sample to excite to electronic energy levels as well as vibrational and rotational energy levels within the electronic excited state. Therefore, absorption

spectroscopy can be used to characterize vibrational and rotational modes of excited states.

The transition from the ground $X\,^2B_1$ state to the $A\,^2A_2$ state of ClO_2 yields an absorption band with its maximum absorbance at ~350 nm (Figure 1). Previous studies have constructed *ab initio* absorption spectra from potential energy surfaces in order to define the vibronic progressions within the absorption band.[12] These studies have found that the large peaks in the spectrum are formed when the symmetric stretch (ν_1) is excited to higher vibrational levels in the excited state. The vibrational level to which each mode is excited is labeled above each peak. These peaks are broadened by the coupling of the symmetric stretch and bend, as well as the coupling of the asymmetric stretch and symmetric stretch.

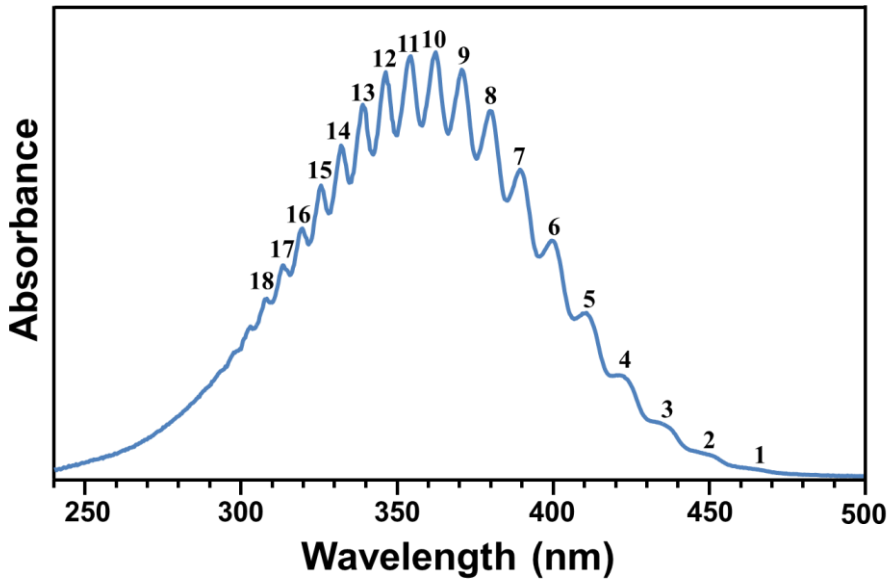

Figure 2. Experimental absorption spectrum of ClO_2 obtained in diethyl ether solution.

Raman Spectroscopy

Raman spectroscopy is a form of vibrational spectroscopy. Instead of the spectrophotometer measuring the percent transmittance of a sample, as in absorption spectroscopy, it measures the amount of light scattered by the sample. If the energy of the incident photon equals the energy of a rotational, vibrational, or electronic transition, the light will be absorbed. If the energies are not equal, the sample will scatter the light either elastically or inelastically (Figure 2). Elastic scattering, known as Rayleigh scattering, occurs when the energy of the scattered light equals the energy of the incident light. This normally happens when the molecule is in a vibrational ground state, is excited to a

virtual state, and then relaxes back to the ground state. Inelastic scattering occurs when the energy of the scattered light does not equal the energy of the incident light. Raman scattering is a type of inelastic scattering and has two possibilities: Stokes scattering and anti-Stokes scattering. Stokes scattering occurs when a sample in its vibrational ground state is excited to a virtual state, but relaxes to an excited vibrational state. Anti-Stokes scattering occurs when a sample already in an excited vibrational state relaxes to its ground state. The differences between the ground and excited vibrational states are displayed as peaks in the Raman spectra. This experiment is performed at room temperature, so the ground state of ClO_2 is more populated than the excited state. Therefore, the peaks in the Raman spectrum will display Stokes scattering.

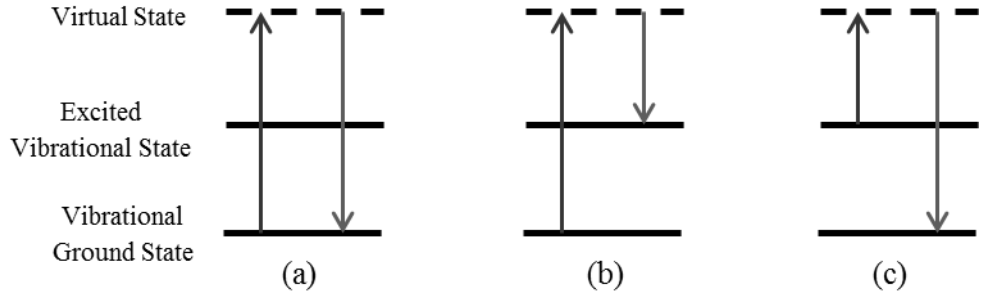

Figure 3. The three forms of scattering are (a) Rayleigh scattering, (b) Stokes scattering, and (c) anti-Stokes scattering.

Experimental Raman spectra of aqueous and gaseous ClO_2 show its fundamental symmetric stretching mode (ν_1) at approximately 945 cm^{-1}. Some experimental spectra of gaseous ClO_2 show the bending mode (ν_3) at 452 cm^{-1}, but the coupling of the symmetric stretch with the bend and the symmetric stretch with the asymmetric stretch decreases the intensity of the bending mode and asymmetric stretching mode to the point where they are not detectable in aqueous solutions.[10] Therefore, many previous experiments have been done to characterize ClO_2 based on changes in ν_1.[11]

When comparing the Raman spectrum to the absorption spectrum of ClO_2, it is first expected that the differences between peaks in the absorption spectrum would equal the value of ν_1 from the Raman spectrum. However, the magnitude of ν_1 is different in in the ground state (ν_1 = 945 cm^{-1}) and the excited state (ν_1 ~700 cm^{-1}) because of the different electronic populations. A Raman spectrum presents a sample's vibrational modes in its ground state, whereas an absorption spectrum presents a sample's vibrational modes in its excited states (Figure 3). The energy difference between the vibrational energy levels is smaller in the excited state than the ground state, which explains why $\nu_{1,\ absorption}$ is smaller than $\nu_{1,Raman}$.

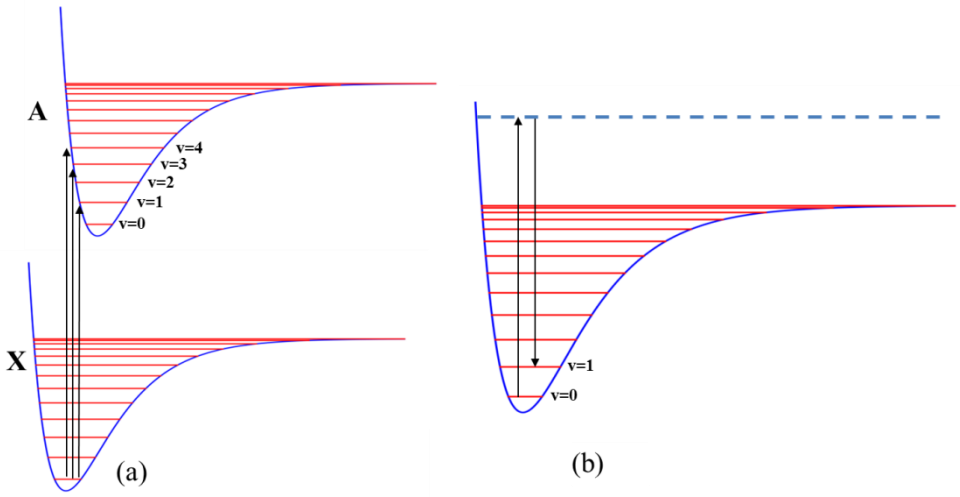

Figure 4. UV-vis absorption spectroscopy and Raman spectroscopy study different energy transitions. (a) UV-vis absorption spectroscopy studies electronic transitions. There are vibrational transitions within each electronic transition. (b) Raman spectroscopy studies vibrational transitions.

Experimental Methods

A design similar to that in Figure 5 should be constructed by the students at the beginning of the laboratory exercise. Chlorine dioxide gas is produced from a reaction between sodium persulfate and sodium chlorite. The yellow gas evolved is bubbled into water, yielding a yellow solution. The chlorine dioxide is then extracted into ether.

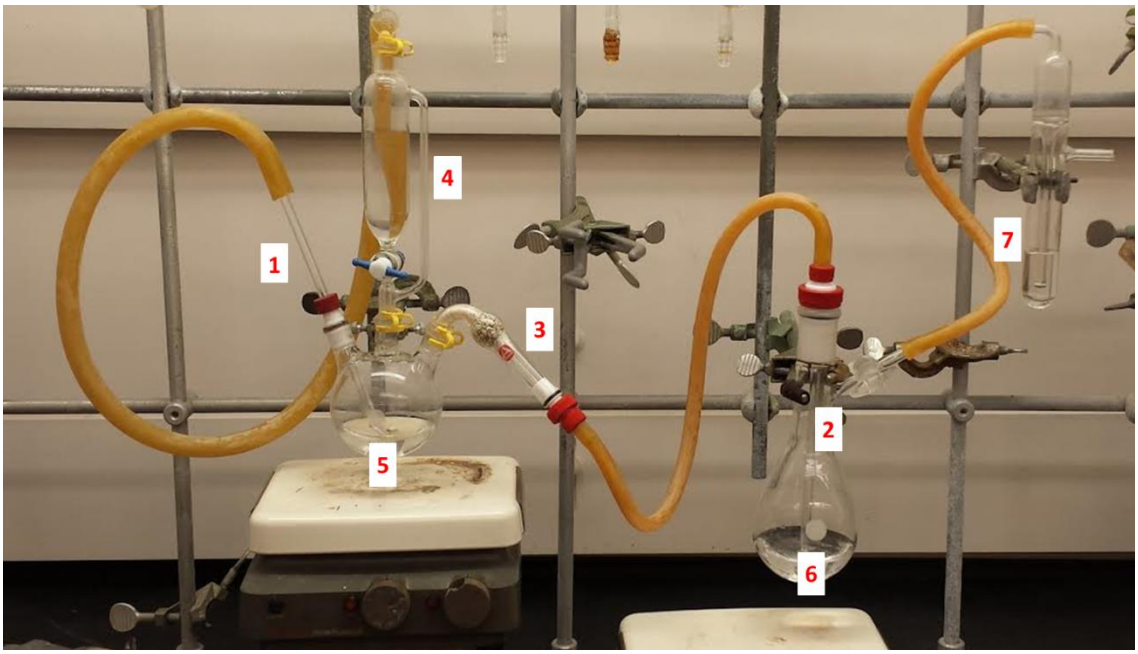

Figure 5. The experimental setup is shown above. The numbers designate the following glassware: (1-3) glass tube, (4) addition funnel, (5) three-neck round bottom flask, (6) Schlenk flask, (7) bubbler.

1) Obtain the following glassware: 250 mL three-necked round bottom flask, 250 mL Schlenk flask, 100 mL addition funnel, and gas inlet adapter. Obtain two small drying tubes and the appropriate sized rubber tubing. Construct a set-up similar to that in Figure 1 using vacuum grease to maintain a vacuum-tight system.
2) A solution of 1.786 g of sodium chlorite dissolved in 50 mL of deionized water is prepared. In order to dissolve all of the sodium chlorite, a stir bar may have to be used. This solution into the 250 mL three-necked round bottom flask, making sure the stirring rod is funneled into the flask with the solution.
3) A solution of 1.597 g of sodium persulfate solution dissolved with stirring in 50 mL of deionized water is prepared. After making sure the stop cock of the addition funnel is securely in the closed position, this solution is added to the 100 mL addition funnel, making sure not to add the stir bar. Close the addition funnel with with a greased stopper.
4) Fill the drying tube with Ascarite. The Ascarite should be tightly packed. Place pieces of cotton at either ends of the tube. Connect the glass tubing from the round-bottom flask to one end of the valve, and place the rubber tubing connected to the other end of the valve to the top of the Schlenk flask.
5) 50 mL of deionized water was added to a 250 mL Schlenk flask equipped with a stir bar. Ensure that the glass tube going in through the top of the flask and the exiting side arm are greased. Position the Schlenk flask so it is almost fully submerged in an ice bath.
6) Fill the bubbler with approximately 25 mL of oil.
7) Connect the glass tube inserted into the sodium chlorite solution to a nitrogen gas tank. Allow a small of nitrogen to flow into the system. Adjust the amount of nitrogen release until the sodium chlorite solution bubbles at a rate of approximately 60 bubbles per minute. The deionized water in the Schlenk flask should bubble as well. If it is not bubbling, examine the system for leaks in the vacuum or restrictions in air flow. Only continue to the next step if both the deionized water and sodium chlorite solutions are bubbling.
8) Allow the sodium persulfate solution to drip into the sodium chlorite solution at a rate of approximately 80 drops per minute.
9) Let the experiment run for one hour. The water in the Schlenk flask should turn yellow, indicating the presence of chlorine dioxide.
10) Turn off the nitrogen gas tank. Separate 10 mL of the chlorine dioxide solution into an Erlenmeyer flask to be evaluated by Raman spectroscopy. Seal the top of the flask with parafilm and wrap the body of the flask in tin foil. The shiny side of the foil should show on the exterior. Store the flask in a cool and dark environment.

11) Pour 15 mL of diethyl ether into the remaining chlorine dioxide solution in the Schlenk flask.

Spectroscopic Methods

A UV-vis absorption spectrum of chlorine dioxide in diethyl ether solution is obtained. The spectrum consists of a single broad absorption peak which displays vibronic progressions. A UV-vis spectrometer that scans over 250 to 500 nm should be used. A Raman spectrum of aqueous chlorine dioxide is also obtained. The symmetric stretching mode should appear in the spectrum as a sharp peak at ~945 cm^{-1}. A Raman spectrometer that has a range of 500 to 1200 cm^{-1} should be used.

1) Pipette approximately 3 mL of the top layer of the chlorine dioxide/ether solution into a quartz cuvette.
2) Obtain the absorbance spectrum of the solution in the cuvette with a UV-vis spectrometer between 250 and 500 nm.
3) Pipette approximately 3 mL of the chlorine dioxide/water solution into a quartz or glass cuvette.
4) Record the vibrational spectrum of the solution in the cuvette with a Raman spectrometer between 500 and 1200 cm^{-1}.
5) Determine ν_1 for the excited state by constructing a Birge-Sponer plot as detailed below using the absorption peaks and compare this value to that obtained for the ground state using Raman spectroscopy.

Presenting Your Spectroscopy Results

Compare your experimental absorption and Raman spectra. Label the vibrational peaks in the absorption spectrum and the symmetric stretching mode in the Raman spectrum. Calculate the difference between the vibrational peaks (in wavenumbers) in the absorption spectrum of as many peaks as you can and compare these values to the value of the symmetric stretching mode in the Raman spectrum. In order to extrapolate ν_1 for the excited state, a Birge-Sponer plot can be constructed.[26] The difference, in wavenumbers, between the discrete vibrational peaks in the UV-vis spectrum ($\Delta\tilde{\nu}(v')$) is plotted against the corresponding vibrational energy level (v'). A linear fit of this graph yields a line with a slope that gives us a measure of the anharmonicity of the vibrational mode and the intercept helps us determine ν_1. Explain why the values obtained for the ground and excited states are different or the same.

ADVANCED OPTION – Computational Methods

The geometry of chlorine dioxide is optimized and its vibrational frequencies in both the ground and excited states can be calculated and compared to the experimental results. A graphical program such as *Gaussview* is used to construct chlorine dioxide, and *Gaussian 09* is used to perform the calculations. A total of three computations are performed. First, the structure of chlorine dioxide is optimized and its frequencies are calculated with the MP2 method and aug-cc-pvtz. The keyword "pop=NBO" is added in the optimization

input file in order to obtain each atom's partial charge. Second, the absorption spectrum is simulated using CIS method and the same basis set. Third, the frequencies of chlorine dioxide in the first excited state are calculated also using the CIS method and the same basis set. Although sample input files are included here for *Gaussian 09*, other software packages can be used as well.

```
%chk=Chlorine_Dioxide.chk
%mem=4GB
%nprocs=2
# MP2/aug-cc-pvtz opt pop=NBO

0 2
Cl
O      1      R
O      1      R      2      A

R 1.6
A 117.6
```

(a)

```
%chk=Chlorine_Dioxide.chk
%mem=4GB
%nprocs=2
# MP2/aug-cc-pvtz freq

0 2
Cl
O      1      R
O      1      R      2      A

R 1.6
A 117.6
```

(b)

Figure 6. (a) A *Gaussian* input file must contain the name of the checkpoint file, the amount of memory that will be allotted for the calculation, the amount of processors that will be allotted for the calculation, and the method and basis set. This example input file employs a z-matrix to define ClO_2's geometry. Starting values of "R" and "A" were found in the literature. The keyword "opt" is added to run an optimization calculation. Once the geometry is optimized according to the method and basis set specified, the values of "R" and "A" will most likely update to the optimized values. Further calculations using the same method and basis set should use the values of "R" and "A" specified in the optimization output file. (b) Another example input file is shown here. The keyword "freq" is added to run a frequency calculation.

Presenting Your Results

Compare the computed absorption spectrum and vibrational frequencies of chlorine dioxide to those obtained experimentally. Explain why the simulated and experimental numbers may be different. What do the NBO results tell you about charge separation in ClO_2?

References

[1] Deshwal, B. R.; Lee, H. K. Manufacture of chlorine dioxide from sodium chlorate: State of the art. *J. Ind. Eng. Chem.* **2005,** *11*, 330-346.

[2] Wang, Y.; Liu, H.; Xie, Y.; Ni, T.; Liu, G. Oxidative removal of diclofenac by chlorine dioxide: Reaction kinetics and mechanism. *Chem. Eng. J.* **2015,** *279*, 409-415.

[3] Friedline, A.; Zachariah, M.; Middaugh, A.; Heiser, M.; Khanna, N.; Vaishampayan, P.; Rice, C. V. Sterilization of hydrogen peroxide resistant bacterial spores with stabilized chlorine dioxide. *AMB Express* **2015,** *5*, 1-6.

[4] Galashev, A. Y., The influence of atmospheric water clusters and halogen ions on ozone depletion. In *Energy, Environment and Economics Research Compendium*, Nova Science Publishers: 2013; pp 279-299.

[5] Tanaka, K.; Tanaka, T. CO_2 and N_2O laser Stark spectroscopy of the ν_1 band of the ClO_2 radical. *J. Mol. Spectrosc.* **1983,** *98*, 425-452.

[6] Hrudey, S. E. Chlorination disinfection by-products, public health risk tradeoffs and me. *Water Res.* **2009,** *43*, 2057-2092.

[7] Rook, J. J. Uproar about chlorine [4]. *Environ. Sci. Technol.* **1975,** *9*, 92-93.

[8] Richardson, S. D.; Plewa, M. J.; Wagner, E. D.; Schoeny, R.; DeMarini, D. M. Occurrence, genotoxicity, and carcinogenicity of regulated and emerging disinfection by-products in drinking water: A review and roadmap for research. *Mutat. Res. Rev. Mutat. Res.* **2007,** *636*, 178-242.

[9] Riesenman, P. J.; Nicholson, W. L. Role of the spore coat layers in Bacillus subtilis spore resistance to hydrogen peroxide, artificial UV-C, UV-B, and solar UV radiation. *Appl. Environ. Microbiol.* **2000,** *66*, 620-626.

[10] Buhr, T. L.; Young, A. A.; Minter, Z. A.; Wells, C. M.; Shegogue, D. A. Decontamination of a hard surface contaminated with Bacillus anthracis Sterne and B. anthracis Ames spores using electrochemically generated liquid-phase chlorine dioxide (e ClO_2). *J. Appl. Microbiol.* **2011,** *111*, 1057-1064.

[11] Foegeding, P. M.; Hemstapat, V.; Giesbrecht, F. G. Chlorine dioxide inactivation of Bacillus and Ciosfridium spores. *J. Food Sci.* **1986,** *51*, 197-201.

[12] Kim, B. R.; Anderson, J. E.; Mueller, S. A.; Gaines, W. A.; Kendall, A. M. Literature review - Efficacy of various disinfectants against Legionella in water systems. *Water Res.* **2002,** *36*, 4433-4444.

[13] Thomsen, C. L.; Reid, P. J.; Keiding, S. R. Quantum yield for ClOO formation following photolysis of aqueous OClO. *J. Am. Chem. Soc.* **2000,** *122*, 12795-12801.

[14] Mahapatra, S.; Krishnan, G. M. Photoelectron spectroscopy of chlorine dioxide and its negative ion: A quantum dynamical study. *J. Chem. Phys.* **2001,** *115*, 6951-6960.

[15] Brooksby, C.; Prezhdo, O. V.; Reid, P. J. Molecular dynamics study of aqueous solvation dynamics following OClO photoexcitation. *J. Chem. Phys.* **2003,** *118*, 4563-4572.

[16] Sun, Z.; Lou, N.; Nyman, G. A $^2A_2 \leftarrow X\ ^2B_1$ absorption and Raman spectra of the OClO molecule: A three-dimensional time-dependent wave packet study. *J. Chem. Phys.* **2005,** *122*.

[17] Esposito, A. P.; Stedl, T.; Jónsson, H.; Reid, P. J.; Peterson, K. A. Absorption and Resonance Raman Study of the $^2B_1(X)-^2A_2(A)$ Transition of Chlorine Dioxide in the Gas Phase. *J. Phys. Chem. A* **1999,** *103*, 1748-1757.

[18] Reid, P. J. Understanding the phase-dependent reactivity of chlorine dioxide using resonance Raman spectroscopy. *Acc. Chem. Res.* **2001,** *34*, 691-698.

[19] Herzberg, G., *Spectra of Diatomic Molecules*. Van Nostrand Reinhold: New York, 1950.

A Spectroscopic Study of the Free Radical Chlorine Dioxide: Faculty Handout

This laboratory focuses on both the synthesis and spectroscopic analysis of the free radical chlorine dioxide (ClO_2). Students first synthesize chlorine dioxide and then analyze its symmetric stretch in both the ground and excited states using Raman and UV-Visible spectroscopies. An optional component includes modeling ClO_2's vibrational frequencies and absorption spectrum using computational chemistry.

Learning Objectives:

(1) Apply techniques for synthesizing inorganic molecules.
(2) Describe the properties of molecular radicals.
(3) Analyze a synthetic product using molecular spectroscopy.
(4) Interpret spectroscopic data to characterize vibrational and electronic energy levels.
(5) Model physical properties using computational chemistry. (optional)

Experimental Methods

A design similar to that in Figure 1 should be constructed by the students at the beginning of the laboratory exercise. The appropriate glassware should be located prior to the laboratory meeting. If glassware shown in Figure 1 is unavailable, substitutions are specified in the Journal. It is important to maintain an air-tight system to optimize product purity and to prevent potentially harmful gaseous ClO_2 leaks.

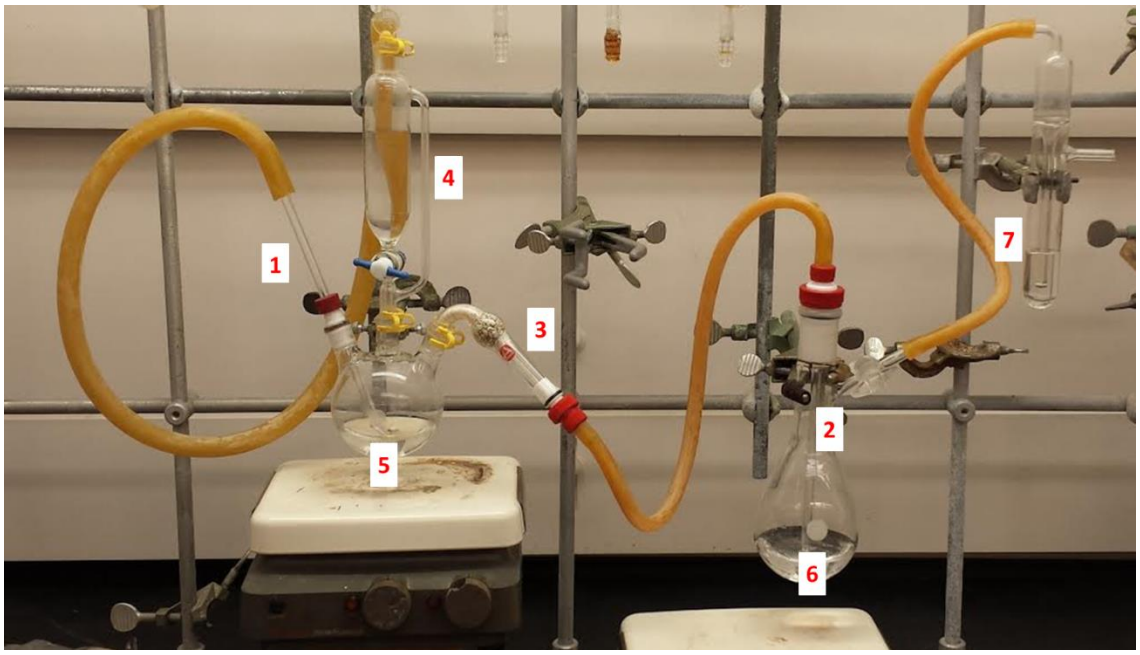

Figure 1. The experimental setup is shown above. The numbers designate the following glassware: (1-3) glass tube, (4) addition funnel, (5) three-neck round bottom flask, (6) Schlenk flask, (7) bubbler.

Spectroscopic Methods

The laboratory exercise should be performed by the instructor prior to the laboratory meeting to specify the appropriate settings for the Raman spectrometer and UV-Vis spectrophotometer.

Computational Methods

As stated in the Results and Discussion section of the Journal, the computed Raman spectra may generated by summing Lorentzian profiles.[31] This can be done using *Microsoft Excel* or a similar spreadsheet.

Hazards

Gaseous ClO_2 is a respiratory and eye irritant. Repeated severe exposure has been shown to irritate eyes and throat, produce nasal discharge, and induce coughing. Delayed-onset pulmonary edema and chronic bronchitis could also occur. Oral consumption can decrease hemoglobin and red blood cell counts. Some studies have shown that prolonged oral consumption is associated with neurotoxicity and depression.[29] ClO_2 cannot be compressed or stored because it decomposes into chlorine and oxygen over time. At high concentrations, gaseous ClO_2 is highly explosive. A concentration of 0.1 ppm is acceptable according to the Occupational Health and Safety Administration[30] and levels here should be far below that. In this laboratory exercise, gaseous ClO_2 is formed at location 5 in Figure 1 and travels to location 6, where it is extracted in aqueous solution. Care must be taken, therefore, to prevent leaks and when extracting the aqueous ClO_2.

References

1. Deshwal, B. R. and H. K. Lee. Manufacture of chlorine dioxide from sodium chlorate: State of the art. *Journal of Industrial and Engineering Chemistry*. **2005**, *113*, 330-346.
2. Wang, Y., H. Liu, et al. Oxidative removal of diclofenac by chlorine dioxide: Reaction kinetics and mechanism. *Chemical Engineering Journal*. **2015**, *279*, 409-415.
3. Friedline, A., M. Zachariah, et al. Sterilization of hydrogen peroxide resistant bacterial spores with stabilized chlorine dioxide. *AMB Express*. **2015**, *51*, 1-6.
4. Galashev, A. Y. The influence of atmospheric water clusters and halogen ions on ozone depletion. *Energy, Environment and Economics Research Compendium*. **2013**, 279-299.
5. Tanaka, K. and T. Tanaka. CO_2 and N_2O laser Stark spectroscopy of the ν_1 band of the ClO_2 radical. *Journal of Molecular Spectroscopy*. **1983**, *982*, 425-452.
6. Brooksby, C., O. V. Prezhdo, et al. Molecular dynamics study of aqueous solvation dynamics following OClO photoexcitation. *Journal of Chemical Physics*. **2003**, *11810*, 4563-4572.
7. Miessler, G. L., P. J. Fischer, et al. *Inorganic Chemistry*, Pearson Education. **2013.**
8. McHale, J. L. Molecular spectroscopy, Pearson College Division.**1999**.
9. Engel, T., P. Reid, et al. *Physical chemistry*. Boston, Pearson. **2013.**

10. Esposito, A. P., T. Stedl, et al. Absorption and Resonance Raman Study of the $^2B_1(X)-^2A_2(A)$ Transition of Chlorine Dioxide in the Gas Phase. *Journal of Physical Chemistry A*. **1999**, *10312*, 1748-1757.

11. Reid, P. J. Understanding the phase-dependent reactivity of chlorine dioxide using resonance Raman spectroscopy. *Accounts of Chemical Research*. **2001**, *349*, 691-698.

12. Sun, Z., N. Lou, et al. $A\ ^2A_2 \leftarrow X\ ^2B_1$ absorption and Raman spectra of the OClO molecule: A three-dimensional time-dependent wave packet study. *Journal of Chemical Physics*. **2005**, *1225*.

13. Richard, E. C. and V. Vaida. The direct near ultraviolet absorption spectrum of the $\tilde{A}\ ^2A_2 \leftarrow \tilde{X}\ ^2B_1$ transition of jet-cooled chlorine dioxide. *Journal of Chemical Physics*. **1991**, *941*, 153-162.

14. Zhang, I. Y., J. Wu, et al. Extending the reliability and applicability of B3LYP. *Chemical Communications*. **2010**, *4618*, 3057-3070.

15. Hofstein, A. and R. Mamlok-Naaman. The laboratory in science education: The state of the art. *Chemistry Education Research and Practice*. **2007**, *82*, 105-107.

16. Williamson, J. C. Teaching the rovibronic spectroscopy of molecular iodine. *Journal of Chemical Education*. **2007**, *848*, 1355-1359.

17. Pursell, C. J. and L. Doezema. The electronic absorption spectrum of molecular iodine: A new fitting procedure for the physical chemistry laboratory. *Journal of Chemical Education*. **1999**, *766*, 839-841.

18. Hollenberg, J. L. Resource papers - VIII. Energy states of molecules. *Journal of Chemical Education*. **1970**, *471*, 2-14.

19. O'Brien, L. C. and R. L. Kubicek. Binding-energy curve for iodine using laser spectroscopy. *Journal of Chemical Education*. **1996**, *731*, 86-87.

20. Muenter, J. S. The Helium-Neon Laser-Induced Fluorescence Spectrum of Molecular Iodine: An Undergraduate Laboratory Experiment. *Journal of Chemical Education*. **1996**, *736*, 576.

21. Pursell, C. J. and L. Doezema. The Electronic Absorption Spectrum of Molecular Iodine: A New Fitting Procedure for the Physical Chemistry Laboratory. *Journal of Chemical Education*. **1999**, *766*, 839.

22. Lessinger, L. Morse Oscillators, Birge-Sponer Extrapolation, and the Electronic Absorption Spectrum of I2. *Journal of Chemical Education*. **1994**, *715*, 388.

23. Galloway, K. R. and S. L. Bretz. Measuring Meaningful Learning in the Undergraduate Chemistry Laboratory: A National, Cross-Sectional Study. *Journal of Chemical Education*. **2015**, *9212*, 2006-2018.

24. Singer, S. and K. A. Smith. Discipline-Based Education Research: Understanding and Improving Learning in Undergraduate Science and Engineering. *Journal of Engineering Education*. **2013**, *1024*, 468-471.

25. Sun, Z., N. Lou, et al. A 2A 2←X 2B 1 absorption and Raman spectra of the OClO molecule: A three-dimensional time-dependent wave packet study. *Journal of Chemical Physics*. **2005**, *1225*.

26. Herzberg, G. *Spectra of Diatomic Molecules*. New York, Van Nostrand Reinhold. **1950.**

27. Frisch, M. J., G. W. Trucks, et al. Gaussian 09. Wallingford, CT, USA, Gaussian, Inc.**2009**.

28. Glendening, E. D., A. E. Reed, et al. NBO Version 3.1.

29. Proctor, N. H., J. P. Hughes, et al. *Proctor and Hughes' chemical hazards of the workplace*, John Wiley & Sons. **2004.**

30. Jin, R.-y., S.-q. Hu, et al. Concentration-dependence of the explosion characteristics of chlorine dioxide gas. *Journal of Hazardous Materials*. **2009**, *1662–3*, 842-847.

31. Scardino, D. J., A. A. Howard, et al. Raman Spectroscopy as the Method of Detection for Constructing a Binary Liquid–Vapor Phase Diagram. *Journal of Chemical Education*. **2011**, *888*, 1162-1165.

32. Esposito, A. P., T. Stedl, et al. Absorption and Resonance Raman Study of the 2B1(X)−2A2(A) Transition of Chlorine Dioxide in the Gas Phase. *The Journal of Physical Chemistry A*. **1999**, *10312*, 1748-1757.
33. Xie, D. and H. Guo. A refined near-equilibrium potential energy surface and the absorption spectrum of OClO(Ã 2A2). *Chemical Physics Letters*. **1999**, *3071-2*, 109-116.
34. Duehr, O., H. Fidder, et al. Ultrafast dynamics of chlorine dioxide in solution upon excitation of the A2A2←X2B1 transition. *IQEC, International Quantum Electronics Conference Proceedings*. **1999**, 77.
35. Peterson, K. A. and H. J. Werner. Multireference configuration interaction calculations of the low-lying electronic states of ClO2. *The Journal of Chemical Physics*. **1992**, *9612*, 8948-8961.
36. Teixeira, O. B. M., V. C. Mota, et al. Single-sheeted double many-body expansion potential energy surface for ground-state ClO2. *Journal of Physical Chemistry A*. **2014**, *11826*, 4851-4862.
37. Wei, Z. Z., B. T. Li, et al. A theoretical investigation of the excited states of OClO radical, cation, and anion using the CASSCF/CASPT2 method. *Journal of Computational Chemistry*. **2007**, *282*, 467-477.
38. Thomsen, C. L., P. J. Reid, et al. Quantum yield for ClOO formation following photolysis of aqueous OClO. *Journal of the American Chemical Society*. **2000**, *12251*, 12795-12801.
39. Riesenman, P. J. and W. L. Nicholson. Role of the spore coat layers in Bacillus subtilis spore resistance to hydrogen peroxide, artificial UV-C, UV-B, and solar UV radiation. *Applied and Environmental Microbiology*. **2000**, *662*, 620-626.
40. Buhr, T. L., A. A. Young, et al. Decontamination of a hard surface contaminated with Bacillus anthracis Sterne and B. anthracis Ames spores using electrochemically generated liquid-phase chlorine dioxide (e ClO_2). *Journal of Applied Microbiology*. **2011**, *1115*, 1057-1064.
41. Foegeding, P. M., V. Hemstapat, et al. Chlorine dioxide inactivation of Bacillus and Ciosfridium spores. *Journal of Food Science*. **1986**, *511*, 197-201.
42. Kim, B. R., J. E. Anderson, et al. Literature review - Efficacy of various disinfectants against Legionella in water systems. *Water Research*. **2002**, *3618*, 4433-4444.
43. Cai, M. Q., L. Q. Zhang, et al. Influencing factors and degradation behavior of propyphenazone and aminopyrine by free chlorine oxidation. *Chemical Engineering Journal*. **2014**, *244*, 188-194.
44. Gibs, J., P. E. Stackelberg, et al. Persistence of pharmaceuticals and other organic compounds in chlorinated drinking water as a function of time. *Science of The Total Environment*. **2007**, *3731*, 240-249.
45. Lee, Y. and U. von Gunten. Oxidative transformation of micropollutants during municipal wastewater treatment: Comparison of kinetic aspects of selective (chlorine, chlorine dioxide, ferrateVI, and ozone) and non-selective oxidants (hydroxyl radical). *Water Research*. **2010**, *442*, 555-566.
46. Barbeau, B., R. Desjardins, et al. Impacts of water quality on chlorine and chlorine dioxide efficacy in natural waters. *Water Research*. **2005**, *3910*, 2024-2033.
47. Pan, Y., W. Li, et al. Formation and occurrence of new polar iodinated disinfection byproducts in drinking water. *Chemosphere*. **2016**, *144*, 2312-2320.
48. Hrudey, S. E. Chlorination disinfection by-products, public health risk tradeoffs and me. *Water Research*. **2009**, *438*, 2057-2092.
49. Rook, J. J. Uproar about chlorine [4]. *Environmental Science and Technology*. **1975**, *92*, 92-93.
50. Richardson, S. D., M. J. Plewa, et al. Occurrence, genotoxicity, and carcinogenicity of regulated and emerging disinfection by-products in drinking water: A review and roadmap for research. *Mutation Research - Reviews in Mutation Research*. **2007**, *6361-3*, 178-242.
51. Wu, M., J. Liu, et al. Effects and kinetics of chlorine dioxide for removal of Benzo[a]pyrene in water. *Environmental Engineering Science*. **2012**, *292*, 133-138.

52. Hrudey, S. E. Chlorination disinfection by-products, public health risk tradeoffs and me. *Water Res.* **2009**, *438*, 2057-2092.
53. Aieta, E. M. and J. D. Berg. A Review of Chlorine Dioxide in Drinking Water Treatment. *Journal (American Water Works Association)*. **1986**, *786*, 62-72.
54. Mahapatra, S. and G. M. Krishnan. Photoelectron spectroscopy of chlorine dioxide and its negative ion: A quantum dynamical study. *Journal of Chemical Physics*. **2001**, *11515*, 6951-6960.
55. Foster, C. E., B. P. Barham, et al. Resonance Raman intensity analysis of chlorine dioxide dissolved in chloroform: The role of nonpolar solvation. *Journal of Chemical Physics*. **2001**, *11419*, 8492-8504.
56. Chorny, I., J. Vieceli, et al. Molecular dynamics study of the vibrational relaxation of OClO in bulk liquids. *Journal of Chemical Physics*. **2002**, *11620*, 8904-8911.
57. Philpott, M. P., S. C. Hayes, et al. Intermolecular hydrogen bonding in chlorine dioxide photochemistry: A time-resolved resonance Raman study. *Chemical Physics*. **2001**, *2632–3*, 389-400.
58. Aguilar, C. A. H., J. Narayanan, et al. Kinetics and mechanism for the oxidation of anilines by ClO2: a combined experimental and computational study. *Journal of Physical Organic Chemistry*. **2014**, *275*, 440-449.
59. Becke, A. D. Density-functional thermochemistry. III. The role of exact exchange. *The Journal of Chemical Physics*. **1993**, *987*, 5648-5652.
60. Hybrid exchange-correlation functional determined from thermochemical data and ab initio potentials. *The Journal of Chemical Physics*. **2001**, *11520*, 9233-9242.
61. Foster, C. E., B. P. Barham, et al. Resonance Raman intensity analysis of chlorine dioxide dissolved in chloroform: The role of nonpolar solvation. *Journal of Chemical Physics*. **2001**, *11419*, 8492.